inorganics

MDPI

Article

Evaluation of DNA and BSA-Binding, Nuclease Activity, and Anticancer Properties of New Cu(II) and Ni(II) Complexes with Quinoline-Derived Sulfonamides

Tamara Liana Topală [1], Ionel Fizeşan [2], Andreea-Elena Petru [2], Alfonso Castiñeiras [3], Andreea Elena Bodoki [1], Luminița Simona Oprean [1], Marcos Escolano [4] and Gloria Alzuet-Piña [5,*]

[1] Department of General and Inorganic Chemistry, Faculty of Pharmacy, "Iuliu Haţieganu" University of Medicine and Pharmacy Cluj-Napoca, 400012 Cluj-Napoca, Romania; topala.liana@umfcluj.ro (T.L.T.); abota@umfcluj.ro (A.E.B.); loprean@umfcluj.ro (L.S.O.)
[2] Department of Toxicology, Faculty of Pharmacy, "Iuliu Haţieganu" University of Medicine and Pharmacy 400012 Cluj-Napoca, Romania; ionel.fizesan@umfcluj.ro (I.F.); andreea.elen.petru@elearn.umfcluj.ro (A.-E.P.)
[3] Department of Inorganic Chemistry, Faculty of Pharmacy, Universidad de Santiago de Compostela, 15705 Santiago de Compostela, Spain; alfonso.castineiras@usc.es
[4] Department of Organic Chemistry, Faculty of Pharmacy, Universitat de València, 46100 Valencia, Spain; marcos.escolano@uv.es
[5] Department of Inorganic Chemistry, Faculty of Pharmacy, Universitat de València, 46100 Valencia, Spain
* Correspondence: gloria.alzuet@uv.es

Abstract: Four complexes of essential metal ions, Cu(II) and Ni(II), with the new sulfonamide ligand *N*-(pyridin-2-ylmethyl)quinoline-8-sulfonamide (HQSMP) were synthesized and physicochemically and structurally characterized. Complex $[Cu(QSMP)Cl]_n$ (**2**) consists of a polymeric chain formed by distorted square pyramidal units. In **two,** the sulfonamide ligand acts as a bridge coordinating to one Cu(II) through its three N atoms and to another metal ion via one O atom in the sulfonamido group, while the pentacoordinate complex $[Cu(QSMP)(C_6H_5COO)]$ (**3**) presents a highly distorted square pyramidal geometry. Complex $[Ni(QSMP)(C_6H_5COO)(CH_3OH)][Ni(QSMP)(CH_3COO)(CH_3OH)]$ (**4**) consists of two mononuclear entities containing different anion coligands, either a benzoate or an acetate group. Both units exhibit a distorted octahedral geometry. The interaction of the complexes with CT-DNA was studied by means of UV-Vis and fluorescence spectroscopy, interestingly revealing that the Ni(II) complex presents the highest affinity towards the nucleic acid. Complexes **1** and **2** are able to cleave DNA. Both compounds show promising nuclease activity at relatively low concentrations by mediating the production of a reactive oxygen species (ROS). The interaction of the four complexes with bovine serum albumin (BSA) was also investigated, showing that the compounds can bind to serum proteins. The antitumor potential of complexes **1** and **2** was evaluated against the A549 lung adenocarcinoma cell line, revealing cytotoxic properties that were both dose- and time-dependent.

Keywords: sulfonamide complexes; transition metal ions; DNA-binding; nuclease activity; anticancer activity; BSA interaction

Citation: Topală, T.L.; Fizeşan, I.; Petru, A.-E.; Castiñeiras, A.; Bodoki, A.E.; Oprean, L.S.; Escolano, M.; Alzuet-Piña, G. Evaluation of DNA and BSA-Binding, Nuclease Activity, and Anticancer Properties of New Cu(II) and Ni(II) Complexes with Quinoline-Derived Sulfonamides. *Inorganics* **2024**, *12*, 158. https://doi.org/10.3390/inorganics12060158

Academic Editor: Christelle Hureau

Received: 23 April 2024
Revised: 25 May 2024
Accepted: 29 May 2024
Published: 1 June 2024

1. Introduction

Medicinal inorganic chemistry is currently an extremely attractive research field due to the high versatility of the studied compounds. With the discovery of the cytotoxic properties of Cisplatin [1] and its incontestable clinical success, drug design entered a new era in which an immense number of metal complexes were synthesized in the hope of overcoming the problems related to the clinical use of this compound, such as low selectivity, resistance, and multiple organ toxicity [2]. Thus, the search for new metal complexes with increased biological activity and specificity for diseased tissues is more

clinically relevant today than it has ever been. Many coordination compounds have proven to be promising candidates for antitumor therapy due to their ability to interact with DNA and their nucleolytic properties; therefore, they are a potential solution to one of the most pressing worldwide public health problems: cancer [3,4].

The interaction of a metal complex with DNA is a crucial step in exerting its biological properties, and it may occur in different ways, depending on the nature of the metal center, the structure of the ligands, and the geometry of the compound [5–7]. As a consequence of this interaction, several structural and conformational changes occur in the nucleic acid molecule, which renders it unable to exert its functions as a carrier of genetic information, ultimately resulting in cell death [8–11].

The potential therapeutic value of metal complexes arises from the complementarity between the properties of the metal ion and the ligand, with the resulting structure often possessing new and interesting properties. They provide the opportunity to exploit the unique properties of metal centers, such as multiple oxidation states, redox properties, a wide variety of coordination numbers, symmetries, and structural patterns, all of which make coordination compounds highly adaptable platforms for drug design [12–17]. Moreover, essential metal ions (including Cu(II) and Ni(II)), naturally occurring in numerous biological structures, show biologically accessible redox potential and a relatively high affinity towards nucleobases [18].

At the same time, the ligands may have pharmacological properties of their own, or they may play a key role in target recognition or interaction, bringing the metal ion near the site where it can exert its function [14,19]. This is the case for sulfonamides, which were the first effective therapeutic agents employed systematically to treat bacterial infections. Nowadays, the known therapeutic properties of this class of compounds are extremely diverse as they are successfully used as diuretics, antidiabetics, anticonvulsants, antivirals, and antiarrhythmics [20–22], with some of them being actively investigated as potential antitumor agents [22–26]. Sulfonamides are also excellent candidates for obtaining metal complexes with diverse biological properties, primarily due to the presence of N and O donor atoms in the sulfonamide group, as well as other functional groups or aromatic structures. Furthermore, it has been proven that their biological activity can be enhanced through metal ion coordination [27].

In developing new pharmacologically active molecules and studying their behavior in the biological environment, it is also very important to understand their interaction with proteins. Investigating the binding mechanism and amplitude of small molecules to serum albumins, the most common proteins in the circulatory system, is crucial in understanding drug pharmacodynamics and pharmacokinetics, as the nature and strength of that interaction have a significant influence on drug absorption, distribution, metabolism, and excretion [28,29].

In recent years, our research group has reported numerous transition metal complexes with sulfonamide ligands that are able to efficiently interact with DNA and mediate its cleavage by generating ROS [9,29–34], including the first case of a Cu-sulfonamide complex acting as a self-activating nuclease [35].

In order to continue our efforts toward developing metallodrugs that are potential candidates for cancer therapy, we have synthesized and thoroughly characterized a new sulfonamide containing the quinoline moiety, *N*-(pyridin-2-ylmethyl)quinoline-8-sulfonamide (HQSMP), and a series of Cu(II) and Ni(II) complexes designed as efficient DNA-binders with nucleolytic properties. The interaction of the coordination compounds with bovine serum albumin (BSA) was also evaluated. We concluded our study by assessing the antitumor potential of two Cu(II) complexes against the A549 lung adenocarcinoma cell line.

2. Results and Discussion

The HQSMP ligand and complexes one, two, three, and four were prepared according to Scheme 1.

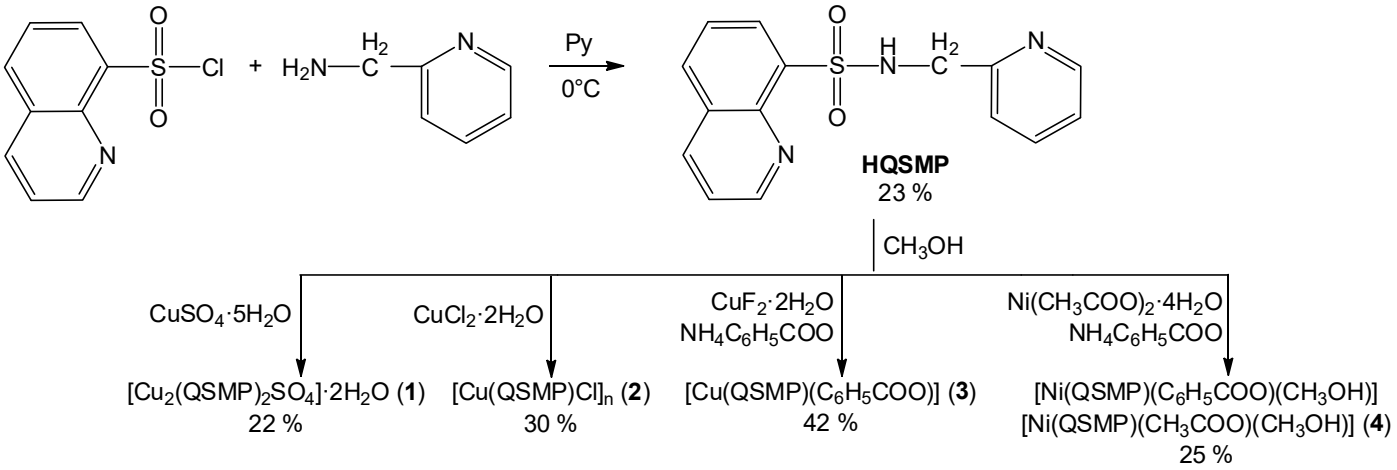

Scheme 1. Synthesis of N-(pyridin-2-ylmethyl)quinoline-8-sulfonamide (HQSMP) and complexes **1**–**4**.

The sulfonamide and the ternary complexes showed good solubility in *N*,*N*-dimethylformamide (DMF) and very low solubility in an aqueous media. They were stable in the solution.

2.1. Crystal Structures

Molecular structures of complexes **2**, **3**, and **4**, including the numbering schemes, are shown in Figures 1–3, while relevant bond distances and angles are comparatively listed in Table 1. The crystals obtained for complex **1** were not of sufficient quality for X-ray diffraction.

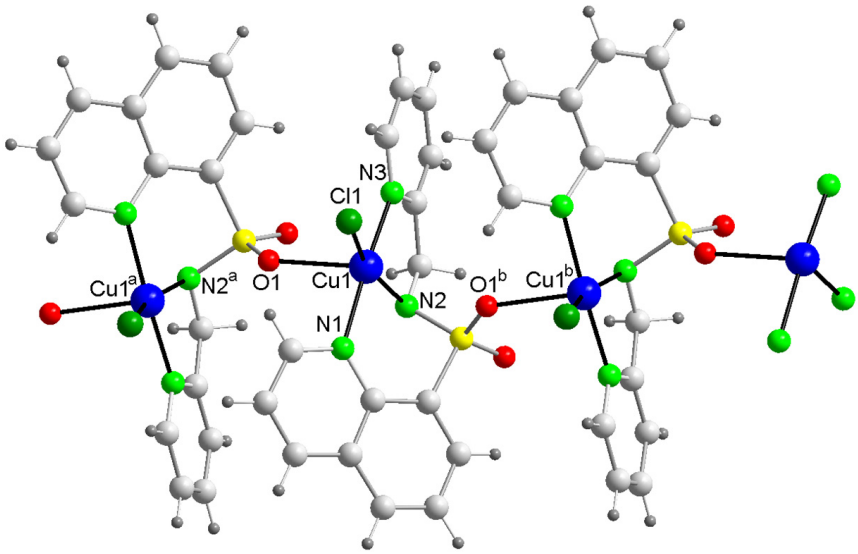

Figure 1. Molecular structure of complex **2**, $[Cu(QSMP)Cl]_n$.

Table 1. Selected bond lengths (Å) and angles (°) for complexes **2**–**4**.

[Cu(QSMP)Cl]$_n$ 2		**[Cu(QSMP)(C_6H_5COO)] 3**		**[Ni(QSMP)(C_6H_5COO)(CH_3OH)] [Ni(QSMP)(CH_3COO)(CH_3OH)] 4**	
Cu(1)-N(1)	2.0494(13)	Cu(1)-N(1)	2.0762(19)	Ni(1)-N(1)	2.119(3)
Cu(1)-N(2)	1.9817(13)	Cu(1)-N(2)	1.9180(19)	Ni(1)-N(2)	2.023(3)
Cu(1)-N(3)	2.0282(13)	Cu(1)-N(3)	1.992(2)	Ni(1)-N(3)	2.044(3)
		Cu(1)-O(21)	1.9414(16)	Ni(1)-O(21)	2.079(2)
		Cu(1)-O(22)	2.5642(18)	Ni(1)-O(22)	2.149(2)
				Ni(1)-O(16)	2.091(2)
Cu(1)-Cl(1)	2.2571(4)				
Cu(1)-O(1)	2.3431(11)				
Cu(1)-Cu(1a)	5.0738(3)				
Cu(1)-Cu(1b)	5.0738(3)				
N(2)-Cu(1)-N(3)	82.37(5)	N(2)-Cu(1)-N(3)	81.88(8)	N(2)-Ni(1)-N(3)	81.89(10)
N(2)-Cu(1)-N(1)	88.81(5)	N(2)-Cu(1)-N(1)	98.33(8)	N(2)-Ni(1)-N(1)	95.85(10)
N(3)-Cu(1)-N(1)	170.88(5)	N(3)-Cu(1)-N(1)	138.68(8)	N(3)-Ni(1)-N(1)	93.07(9)
		O(21)-Cu(1)-N(1)	95.12(7)	O(21)-Ni(1)-N(1)	98.17(10)
		N(2)-Cu(1)-O(22)	108.61(7)	N(2)-Ni(1)-O(22)	103.32(10)
		O(21)-Cu(1)-O(22)	56.74(6)	O(21)-Ni(1)-O(22)	62.60(9)
		N(3)-Cu(1)-O(22)	108.79(7)	N(3)-Ni(1)-O(22)	87.79(9)
		N(1)-Cu(1)-O(22)	110.12(7)	N(1)-Ni(1)-O(22)	160.73(9)
		N(2)-Cu(1)-O(21)	163.13(7)	N(2)-Ni(1)-O(21)	165.73(9)
		O(21)-Cu(1)-N(3)	94.68(8)	N(3)-Ni(1)-O(21)	94.68(10)
				N(2)-Ni(1)-O(16)	90.87(9)
				N(3)-Ni(1)-O(16)	169.81(9)
				O(21)-Ni(1)-O(16)	90.59(9)
				O(16)-Ni(1)-N(1)	94.81(9)
				O(16)-Ni(1)-O(22)	86.91(9)
N(1)-Cu(1)-O(1)	85.87(5)				
Cl(1)-Cu(1)-O(1)	96.31(3)				
N(2)-Cu(1)-Cl(1)	161.82(4)				
N(3)-Cu(1)-Cl(1)	95.53(4)				
N(1)-Cu(1)-Cl(1)	93.58(4)				
N(2)-Cu(1)-O(1)	101.84(5)				
N(3)-Cu(1)-O(1)	93.61(5)				

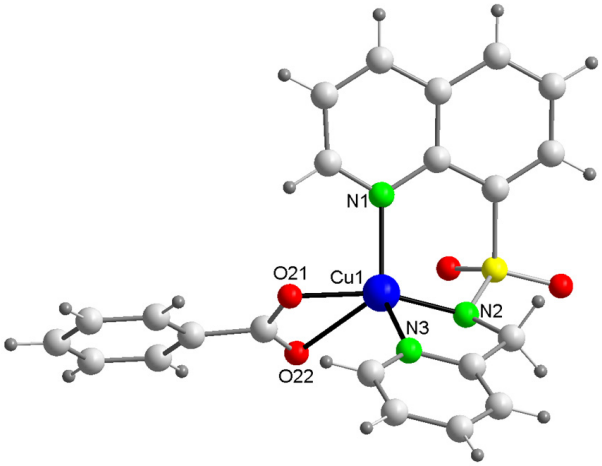

Figure 2. Molecular structure of complex **3** [Cu(QSMP)(C_6H_5COO)].

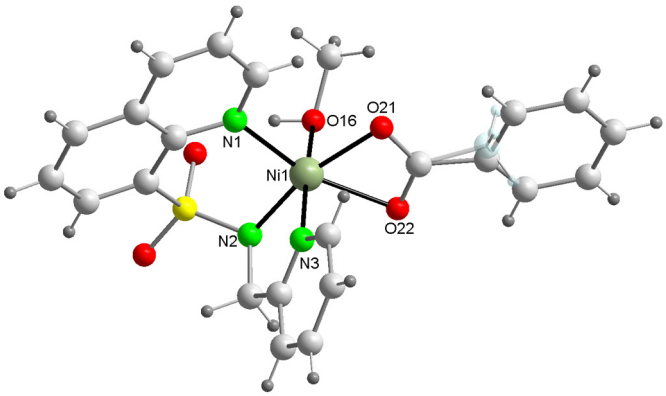

Figure 3. Molecular structure of complex **4**: [Ni(QSMP)(C_6H_5COO)(CH_3OH)][Ni(QSMP)(CH_3COO)(CH_3OH)].

[Cu(QSMP)Cl]$_n$ (2)

In complex 2 (Figure 1), the local environment of the metal center corresponded to a distorted square pyramid with a CuN_3ClO chromophore.

In order to evaluate the degree of distortion of the coordination polyhedron, the τ structural index parameter proposed by Addison et al. [36] was calculated. This parameter characterizes five-coordinated systems as an index of the degree of trigonality within the range of structural possibilities between the ideal trigonal bipyramidal and square pyramidal geometries. The geometric parameter was defined as $\tau = (\beta - \alpha)/60$, where α and β were the largest angles formed with the metal center in the coordination polyhedron. For a perfect square pyramidal geometry, τ = 0, while for an ideal trigonal bipyramid, τ = 1. In the case of complex 2, the value of the distortion parameter, τ = 0,15,1, indicated that the coordination geometry of the metal ion was a slightly distorted square pyramidal.

The equatorial plane was defined by the three N atoms belonging to the sulfonamide: N-quinoline [N(1)], N-sulfonamide [N(2)], and N-pyridyl atoms [N(3)] and the chloride anion. The axial position was occupied by one O atom [O(1)], pertaining to the sulfonamide group of the ligand from the neighboring complex unit, creating a polymeric chain. The Cu-N bond lengths that fell within the 1.9817(13) Å–2.0494(13) Å range were consistent with similar structures containing the pyridyl and quinoline moieties [37,38]. The chloride anion formed a 2.2571(4) Å bond with the metal center, similar to the Cu-Cl previously reported bond lengths [29]. These equatorial distances were, as usual, shorter than the axial one, Cu-O(1) 2.3431(11) Å. The distance between two Cu(II) ions in the polymeric chain was 5.0738(3) Å.

The cis and trans angles formed by the metal center with the equatorial atoms also differed significantly from the ideal value and were in the range of 82.37(5)°–102.65(3)° and 170,88 (5)°–161.82 (4)°, respectively, which is to be expected for a highly distorted geometry.

[Cu(QSMP)(C_6H_5COO)] (3)

Cu(II) in complex 3 was also five-coordinated (Figure 2). The τ structural index of 0.407 indicates that the coordination geometry of the metal ion was almost half-way between the square pyramidal and trigonal bipyramidal [36].

In the coordination polyhedron, four shorter bonds could be identified, ranging from 1.9180(19) Å to 2.0762(19) Å, formed by the three nitrogen atoms belonging to the sulfonamide ligand [N(1), N(2), N(3)] and one of the oxygen atoms of the benzoate coligand [O(21)]. The fifth position was defined by the longest bond, formed with the second O-carboxylate atom [Cu-O(22) 2.5642(18) Å]. The difference in length between the two Cu(II)-O-carboxylate bonds was remarkable (0.6228 Å), a phenomenon previously encountered for bidentate carboxylates [39,40].

The extent of the distortion of the square pyramidal geometry was also reflected by the angles in the coordination polyhedron. The angles formed by the atoms in trans positions

severely deviated from 180° [N(2)-Cu-O(21) 163.13(7)°, N(3)-Cu-N(1) 138.68(8)°], while the angles formed by the atoms in cis positions fell within the range of 56.74(6)°–110.12(7)°, the smallest angle being the one formed by the two O-carboxylate atoms with the metal ion, as seen in other complexes containing this anion as a bidentate ligand [29,39].

[Ni(QSMP)(C6H5COO)(CH3OH)][Ni(QSMP)(CH3COO)(CH3OH)] (4)

The crystal structure of complex 4 consisted of two mononuclear Ni(II) entities (Figure 3). The metal ion showed similar coordination environments, the difference being one of the coligands. Entity I contained a benzoate moiety, while entity II incorporated an acetate group. Both Ni(II) ions showed a distorted octahedral geometry, with a NiN_3O_3 chromophore and identical bonds and angles formed within the coordination polyhedron.

The sulfonamide acted, as in complex 3 as a tridentate ligand, coordinating the metal ion through its three N atoms, N-pyridyl (axial position), N-sulfonamide, and N-quinoline (equatorial positions), forming stable five- and six-membered rings. The remaining equatorial positions were occupied by the two oxygen atoms corresponding to the carboxyl groups (benzoate in entity I and acetate in entity II), both acting as bidentate. The sixth position of the octahedron (and the second axial position) was claimed by an oxygen atom belonging to a methanol molecule.

The length of the bonds formed by the Ni(II) ion with the atoms in trans positions were very similar: Ni-O(16) 2.091(2) Å and Ni-N(3) 2.044(3) Å; Ni-O(21) 2.079(2) Å and Ni-N(2) 2.023(3) Å; Ni-N(1) 2.119(3) Å and Ni-O(2) 2.149(2) Å. As can be observed, the two Ni-O-carboxylate bond lengths were slightly different, as expected for this coordination mode of the carboxylate group. The Ni-N-pyridyl, Ni-N-sulfonamido, and Ni-N-quinoline bond lengths fell within the normal range for this type of structure [41–43].

The distortion of the octahedron could also be noted from the values of the angles formed by the atoms in cis positions with the central metal ion, as they deviated significantly from 90° and were in the range of 62.60(9)°–103.32(10)°. Similarly to the situation encountered in complex 3, the largest deviation from a regular octahedron was the angle formed with the two carboxylate oxygen atoms as a consequence of the double coordination.

Intermolecular interactions

A series of intermolecular interactions contributed to the stabilization of the complex structures. Weak-to-medium strength quinoline–quinoline π-π interactions were observed in complexes 2, 3, and 4. The aromatic structures were positioned in a parallel manner or formed a very small dihedral angle (α = 1.483°), while the β and γ displacement angles indicated a pronounced slipping of the interacting rings, as they had values ranging from 22.13° to 30.25°. In the case of complex 4, the distances between the quinoline and phenyl moieties (3.6557 Å–3.8663 Å) were also indicative of medium-strength or weak π-π stacking interactions [44].

For complexes 2 and 4, edge-to-face C-H. . .π interactions were also observed. In the case of complex 2, one of the *meta*-H atoms of the pyridine moiety pointed towards one ring of the coordinated quinoline belonging to an adjacent complex molecule, while for complex 4, the interactions involved the H(5) atom, which pointed towards the center of the pyridine ring belonging to the neighboring complex molecule.

The structures of complexes 3 and 4 were further stabilized by intra- and intermolecular hydrogen bridges and bonds of moderate strength [45].

The geometric parameters characterizing the above-described interactions are summarized in Tables 2 and 3. Ring interactions were taken into consideration for distances between centroids of less than 6 Å and slipping angles inferior to 60°. C-H. . .π interactions were taken into consideration for distances between hydrogen atoms and centroids of less than 3 Å and γ angles inferior to 30°.

Table 2. Geometric parameters for π-π stacking interactions for complexes 2–4.

π-π stacking	d_{Cg-Cg} (Å)	D ⊥ [Cg(I)-P(J)] (Å)	D ⊥ [Cg(J)-P(I)] (Å)	α (°)	β (°)	γ (°)
2						
quinoline–quinoline						
Cg(1)-Cg(1) [a]	3.6187	3.3521	3.3521	0	22.13	22.13
Cg(1)-Cg(3) [a]	3.8523	3.3278	3.3519	1.483	29.53	30.25
3						
quinoline–quinoline						
Cg(8)-Cg(8) [b]	3.6343	3.3430	3.3430	0	23.09	23.09
4						
quinoline–quinoline						
Cg(9)-Cg(9) [c]	3.8925	3.4469	3.4469	0	27.68	27.68
quinoline–phenyl						
Cg(7)-Cg(10) [d]	3.6558	3.4068	3.3378	5.534	24.07	21.27
Cg(9)-Cg(10) [d]	3.8342	3.1372	3.3976	7.513	27.61	35.09

d_{Cg-Cg}: distance between ring centroids; α: dihedral angle formed by the rings; β, γ: slipping angles; d ⊥ [Cg(I)-P(J)]: distance between centroid Cg(I) and plane J; d ⊥ [Cg(J)-P(I)]: distance between centroid Cg(J) and plane I; [a] 1 − x, 1 − y, 1 − z; [b] 1 − x, 1 − y, -z; [c] 1 − x, −y, −z; [d] 1/2 + x, 1/2 − y, 1/2 + z **2**: Cg(1): N1-C1-C2-C3-C4-C9; Cg(3): C4-C5-C6-C7-C8-C9; **3**: Cg(8): C4-C5-C6-C7-C8-C9; **4**: Cg(7): N1-C1-C2-C3-C4-C9; Cg(9): C4-C5-C6-C7-C8-C9; Cg(10): C22-C23-C24-C25-C26-C27.

Table 3. Geometric parameters for C-H. . .π interactions in complexes **2** and **4**.

C-H. . .π Interactions	d_{H-Cg} (Å)	D ⊥ [H-P(I)] (Å)	d_{C-Cg} (Å)	<[C-H. . .P(I)] (°)	γ (°)
2					
C12-H12 . . . Cg(3) [a]	2.85	2.83	3.5305	130	6.49
4					
C5-H5 . . . Cg(8) [b]	2.99	2.83	3.7028	132	19.06

d_{H-Cg}: distance between the H atom and the ring centroid; d ⊥ [H-P(I)]: distance between the H atom and the ring plane; d_{C-Cg}: distance between the C atom and the ring centroid; <[C-H. . .P(I)]: angle formed by the C and H atoms and the ring centroid; **2**: [a] −x, −1/2 + y, 1/2 − z; Cg(3): C4-C5-C6-C7-C8-C9; **4**: [b] 1 − x, −y, −z; Cg(8):N3-C11-C12-C13-C14-C15.

2.2. Spectroscopic Properties and Complex Stability in Solution

The complexes show IR spectra with a similar pattern, the most notable feature being the disappearance of the band assigned to the N-H stretching vibration, indicating the deprotonation of the sulfonamide upon coordination (Figure S1). As a consequence of the involvement of the sulfonamide moiety in coordinating the metal center and/or its deprotonation, the bands assigned to $\nu_{asym}(SO_2)$, $\nu_{sym}(SO_2)$, and ν(S-N) appeared to shift in the IR spectra of the complexes in a similar way to the changes observed in the IR spectra of related compounds (Figure S1) [9,29,30,35].

Additional bands appeared in the IR spectra of complexes **1, 3,** and **4** due to the presence of the coligands. The bands at 1055, 1024, 997, and 608, in the case of complex **1**, corresponded to the asymmetry bending and symmetry stretching vibrations of the SO_4^{2-} group in accordance with a bridging bidentate sulfato moiety [46,47]. The IR spectra of complexes **3** and **4** exhibited bands corresponding to the COO^- group. The $\nu_{asym}(COO^-)$ and $\nu_{sym}(COO^-)$ appeared at 1563 cm^{-1} and 1519 cm^{-1} and at 1441 cm^{-1} and 1418 cm^{-1}, respectively. The value of Δ [$\Delta = \nu_{asym}(COO^-) - \nu_{sym}(COO^-)$], equal to 101 cm^{-1} for complex **3** and 122 cm^{-1} for complex **4**, was consistent with the coordination mode of the carboxylate anion, which acted as a bidentate ligand in both complexes [39,46]. The medium intensity broad band at 3262 cm^{-1} in the spectrum of complex **4** was attributed to the methanol molecule, acting as a coligand [29].

The UV-Vis spectra were recorded in a solid state and in DMF solution for all complexes (Figure S2). The diffuse reflectance spectrum corresponding to complex **one** exhibited a

wide asymmetrical *d-d* transition band centered at 730 nm, while the band at 325 nm was assigned to charge transfer transitions. Complex **2** showed a broad band at 735 nm, characteristic of a distorted octahedral geometry, and a shoulder at 380 nm, which was attributed to charge transfer transitions, while the spectrum of complex **3** exhibited a CT shoulder at 395 nm and a *d-d* band centered at 700 nm, consistent with a five-coordinate structure [48]. In the spectrum of complex **4,** a broad *d-d* transition band centered at 640 nm was identified, in agreement with the octahedral geometry of the local environment, and a type NiN_3O_3 chromophore [49], while the band exhibited at 330 nm was assigned to charge transfer transitions.

In a DMF solution, all complexes showed similar spectrum patterns to those obtained in a solid state. Their electronic spectra exhibited well-defined bands or shoulders in the range of 316–408 nm and broad, asymmetric ligand field bands in the 630–723 nm region of the visible spectrum (Figure S2). In a solution, the bands appeared to shift with respect to the diffuse reflectance spectra of the complexes, indicating possible coordination by solvent molecules [34]. All three Cu(II) complexes showed evidence of charge transfer transitions, as their electronic spectra exhibited well-defined bands or shoulders in the range of 316–408 nm, while the *d-d* transitions appeared as broad, asymmetric bands in the 685–723 nm region. The spectrum of complex **4** showed a CT shoulder at 318 nm and a *d-d* band centered at about 630 nm. No modifications were observed in the UV-Vis spectra for a period of several weeks, indicating the stability of the complexes in the solution.

Moreover, the ESI^+ mass spectra of complexes **1**–**4** confirmed the stability of the ternary structures in the solution, showing *m*/*z* peaks at 821.0, 398.7, 482.7, 489.3, and 510.1, corresponding to $[Cu_2(QSMP)_2SO_4 + H^+]^+$, $[Cu(QSMP)Cl + H^+]^+$, $[Cu(QSMP)(C_6H_5COO) + H^+]^+$, $[Ni(QSMP)(CH_3COO)(CH_3OH) + K^+]^+$, and $[Ni(QSMP)(C_6H_5COO)(CH_3OH) + H^+]^+$, respectively.

Taking into account the fact that, for complex **1**, the crystal structure could not be determined by means of X-ray diffraction, a molecular formula was proposed based on the ESI^+ mass spectra; the changes observed in the IR bands corresponded to the ligand, which was similar to those seen for the other complexes as well as the bands attributed to the SO_4^{2-} group, with the ligand acting as a tridentate and containing the bridging bidentate sulfato group.

2.3. DNA-Binding Studies

2.3.1. Thermal Denaturation

The interaction of the complexes with CT-DNA was investigated by observing the changes in the melting temperature (Tm) of the nucleic acid, which was considered to be the temperature at which half of the nucleic acid was found in the double-stranded state and the other half in a single-stranded form [8,50]. The results are shown in Table 4 (and Figure S3). All compounds increased the melting temperature of the DNA, a phenomenon indicative of an interaction with the nucleic acid, stabilizing its structure. The ΔTm values obtained were 6.6, 7, 5.3, and 10.9 °C for compounds **1**–**4**, respectively, allowing us to conclude that the affinity of the complexes towards DNA follows the order of **3** < **1** ≈ **2** < **4**. Furthermore, the moderate increase in the DNA melting temperature in the case of complexes **1**–**3** may indicate a groove binding type of interaction with the nucleic acid, while the rather high value obtained for the Ni(II) complex suggests a possible intercalative binding [29]. An interesting observation is that the higher DNA affinity of the Ni(II) complex than the Cu(II) complexes was similar to what was observed in the case of other series of coordination compounds involving similar sulfonamide derivatives [29] and also other types of ligands [51].

Table 4. ΔTm of CT-DNA and fluorescence quenching parameters of EB-DNA adduct in the presence of complexes **1**–**4**.

Complex	ΔTm (°C)[a]	% Hypochromism	K_{SV} (M^{-1})
1	6.6	20.9	-
2	7	14.8	2.32×10^3
3	5.3	16.2	-
4	10.9	34.6	6.58×10^3

[a] [DNA]/[complex] = 2 (**1**, **2** and **3**); [DNA]/[complex] = 4 (**4**).

2.3.2. Ethidium Bromide Displacement Assay

To obtain a better understanding of the interaction of the complexes with DNA, the affinity of the complexes towards CT-DNA was also investigated by means of fluorescence spectroscopy. Changes in the emission intensity of the ethidium bromide (EB) bound to DNA in the presence of the complexes were monitored. When intercalated between DNA base pairs, EB showed a significant increase in emission intensity with respect to the free form of the dye due to steric protection provided by the nucleobases [52]. The presence of another compound (such as a metal complex) may be translated into a decrease in the emission intensity as a result of its interaction with the EB-DNA adduct. This phenomenon could be the consequence of several possible processes, such as the displacement of the EB molecule from its binding sites due to the competitive binding of the metal complex, a photoelectron transfer from the EB in the excited state to the metal ions, or a conformational change in the DNA molecule as a result of the interaction of the metal complex with the nucleic acid, resulting in the exposure of EB to solvent and O_2 molecules and the subsequent deactivation of its excited state [35,53].

As shown in Table 4 and Figure 4, in all cases, the presence of the complexes led to a decrease in the emission intensity characteristic in the EB-DNA adduct in a concentration-dependent manner. The degree to which the fluorescence of the EB-DNA system was quenched by the addition of the complexes (hypochromism calculated for the emission maximum) increased in the order of **2** ≈ **3** < **1** < **4**, with a moderate decrease in fluorescence intensity in the presence of complexes **2** and **3** (≈15%) and a more considerable quenching observed for complex **4** (34%). Interestingly, the results indicate that the Ni(II) complex had the highest binding affinity towards DNA, which was in agreement with the data provided by the thermal denaturation studies. This type of behavior was previously reported by our group, showing that Ni(II) complexes appear to interact stronger with the nucleic acid than analogous Cu(II) complexes with similar structures [29].

The experimental data were analyzed using the Stern–Volmer equation [53]:

$$I_0/I = 1 + K_{SV}[Q] \quad (1)$$

where I_0 and I are the fluorescence intensities of the EB-DNA adduct in the absence and in the presence of the quencher, respectively, K_{SV} is the Stern–Volmer quenching constant, and [Q] is the concentration of the quencher.

For complexes **2** and **4**, the plots I_0/I vs. [Complex] for the quenching of the EB-DNA fluorescence were in good agreement with the linear Stern–Volmer equation, with K_{SV} values of 2.32×10^3 M^{-1} and 6.65×10^3 M^{-1}, respectively. The results once again confirm that the Ni(II) complex was the one with the highest affinity for the nucleic acid. The K_{SV} values were of the same order of magnitude as the transition metal complexes with ligands containing aromatic structures that were previously reported [29,35], indicating an overall moderate affinity for DNA. The deviation from linearity observed for complexes **1** and **3** did not allow the calculation of the K_{SV} constants, but the decrease in the emission intensity of the EB bound to the DNA in the presence of these complexes indicated their interaction with the nucleic acid.

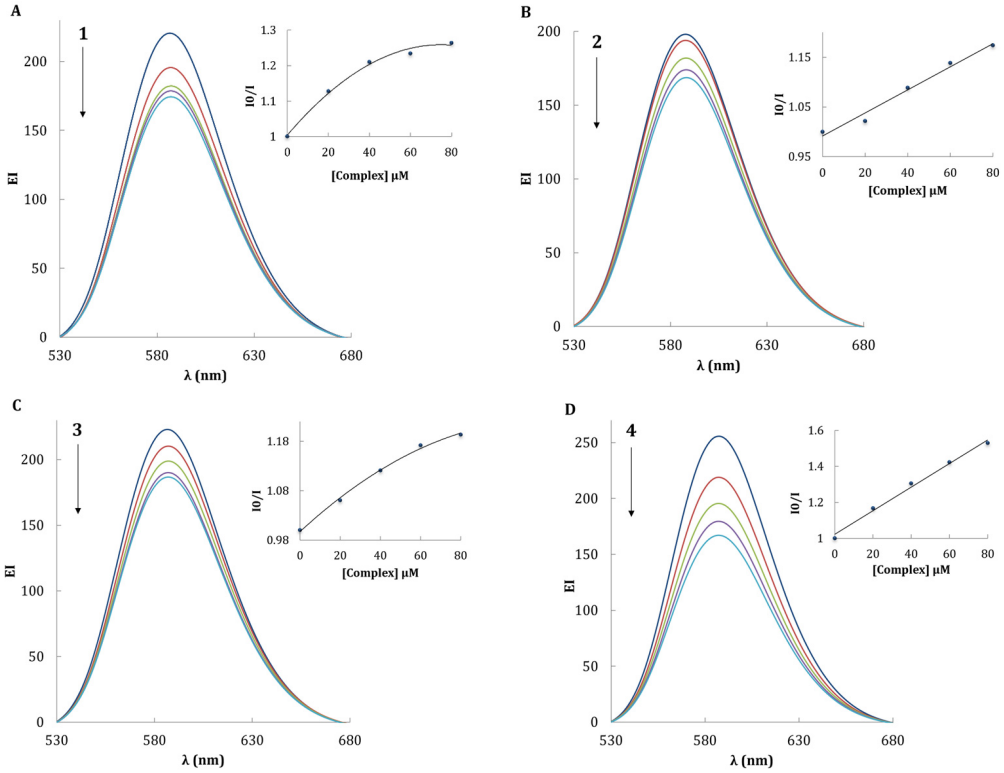

Figure 4. Emission spectra of EB bound to DNA in the absence and presence of increasing concentrations of **1** (**A**), **2** (**B**), **3** (**C**) and **4** (**D**) The arrow shows the changes in intensity at increasing concentrations of the complex (20-80 μM). Inset: Stern–Volmer plot.

2.4. DNA Cleavage and Mechanistic Studies

2.4.1. DNA Cleavage in the Presence of Ascorbate

The ability of the Cu(II) complexes to damage supercoiled pUC18 DNA was investigated by means of gel electrophoresis in the presence of ascorbate at the same concentration as the complex as an activating agent. The potency of the complexes as chemical nucleases was evaluated as the extent of the conversion of supercoiled DNA (SC-DNA, form I) to its open circular (OC-DNA, form II) and linear conformations (L-DNA, form III), in comparison with the nucleolytic properties of Cu(II) in the same experimental conditions. As shown in Figure 5A, the Cu(II) ion failed to cleave the DNA. Complexes **1** and **2** behaved in a very similar fashion regarding their nucleolytic abilities (Figure 5B and 5C, respectively), cleaving DNA in a concentration-dependent manner. At a concentration of 20 μM, both complexes were able to partially convert SC-DNA (Form I) to OC-DNA (Form II) (lanes 3B and 3C) as a result of a single strand scission unraveling the supercoiled DNA. In the case of complex **2**, small amounts of L-DNA (Form III) appeared at a 25 μM complex concentration (lane 4C), indicating that a second scission occurred on the complementary strand within about twelve base pairs from the first one [13]. In the case of complex **3,** the results indicated that it did not efficiently cleave pUC18 plasmid DNA at the assayed concentration range and under the given experimental conditions. Since Ni(II) compounds are known for their ability to perform DNA cleavage following a hydrolytic mechanism [13,54], we have studied the nuclease activity of complex **4** in the absence of reducing agents. Unfortunately, **4** was not able to cleavage the DNA.

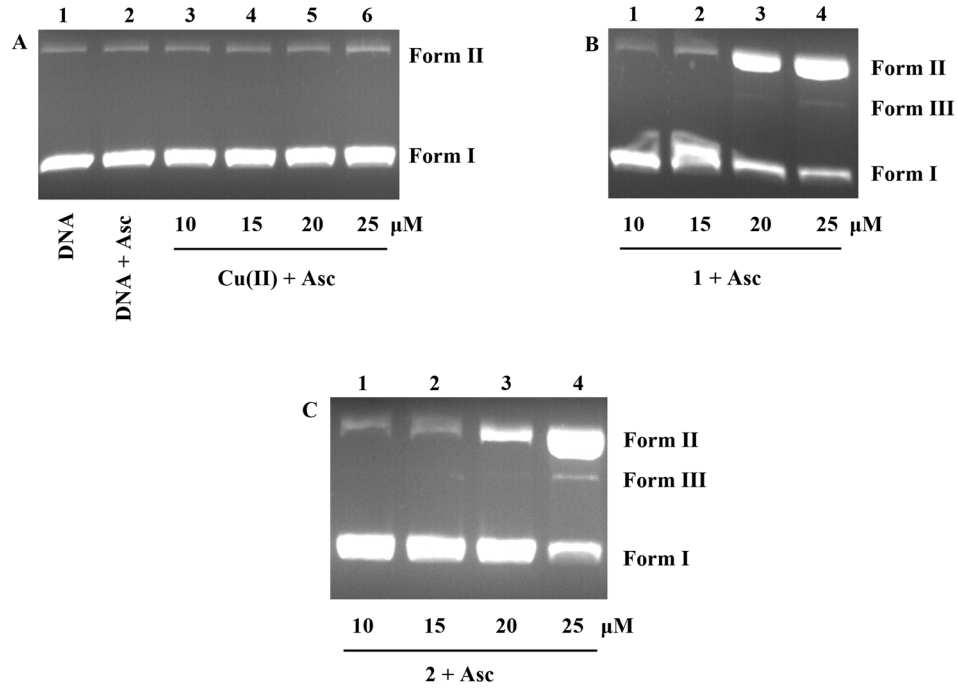

Figure 5. Agarose gel electrophoresis of pUC18 DNA treated with Cu(II) (**A**) and complexes **1** (**B**) and **2** (**C**) in the presence of 1-fold molar excess of ascorbate (1×). Lanes: 1A. pUC18 DNA control; 2A. pUC18 DNA + ascorbate 25 µM; 3A-6A. Cu(II) + ascorbate 10–25 µM; 1B–4B. complex **1** + ascorbate (1×); 1C–4C. complex **2** + ascorbate (1×); 1C–4C.

2.4.2. Mechanistic Studies

In order to investigate the mechanism followed by complexes **1** and **2** in inflicting DNA damage and highlight the species involved in the strand scission, we performed gel electrophoresis in the presence of known quenchers of the nucleolytic process. As most transition metal complexes follow an oxidative mechanism in exerting their nuclease activity, the involvement of ROS was tested in the presence of scavengers. Neocuproine, a Cu(I) chelator, was also used to further clarify the cleavage mechanism. Furthermore, the groove binding ability of the complexes was evaluated in the presence of Hoechst (minor groove binder) and methyl green (major groove binder). The studies were conducted with complexes **1** and **2** at 25 µM. Results are presented in Figure 6.

In the presence of sodium formate, KI, and DMSO, a decrease in the nuclease potency of both complexes was observed (lanes 2A–4A and 2B–4B), suggesting the involvement of the hydroxyl radical in the DNA damage. The apparent higher inhibition of the nucleolytic process by KI (lanes 3A and 3B) could be explained by the fact that it also interacted with the Cu(I) ion, forming the stable cuprous iodide [55]. The presence of superoxide scavenger Tiron completely inhibited the DNA strand scission in the case of both complexes (lanes 6A and 7B), indicating that superoxide was one of those responsible for the pUC18 damage. The addition of D_2O did not influence the nucleolytic process in either case (lanes 5A and 6B), suggesting that neither a singlet oxygen nor singlet-oxygen-like species intervened. Neocuproine, a Cu(I) chelator, significantly decreased the DNA cleavage mediated by both complexes (lane 8A and 8B) as a consequence of the Cu(I) depletion from the reaction mixture, a fact that indicates that the reduction in the central Cu(II) ion was a key step in generating ROS. In order to collect additional information regarding the type of interaction between the DNA double helix and complexes **1** and **2**, the influence of groove binders on the nucleolytic process was also studied. The major groove binder methyl green did not have an influence on the nuclease activity of the complexes (lanes 7A and 5B). In the presence of the minor groove binder Hoechst, a moderate decrease in the damage induced by complex **1** (lane 9A) was found, while a complete inhibition of the process was

observed in the case of complex **2** (lane 9B), suggesting that the compounds exhibited a minor groove preference.

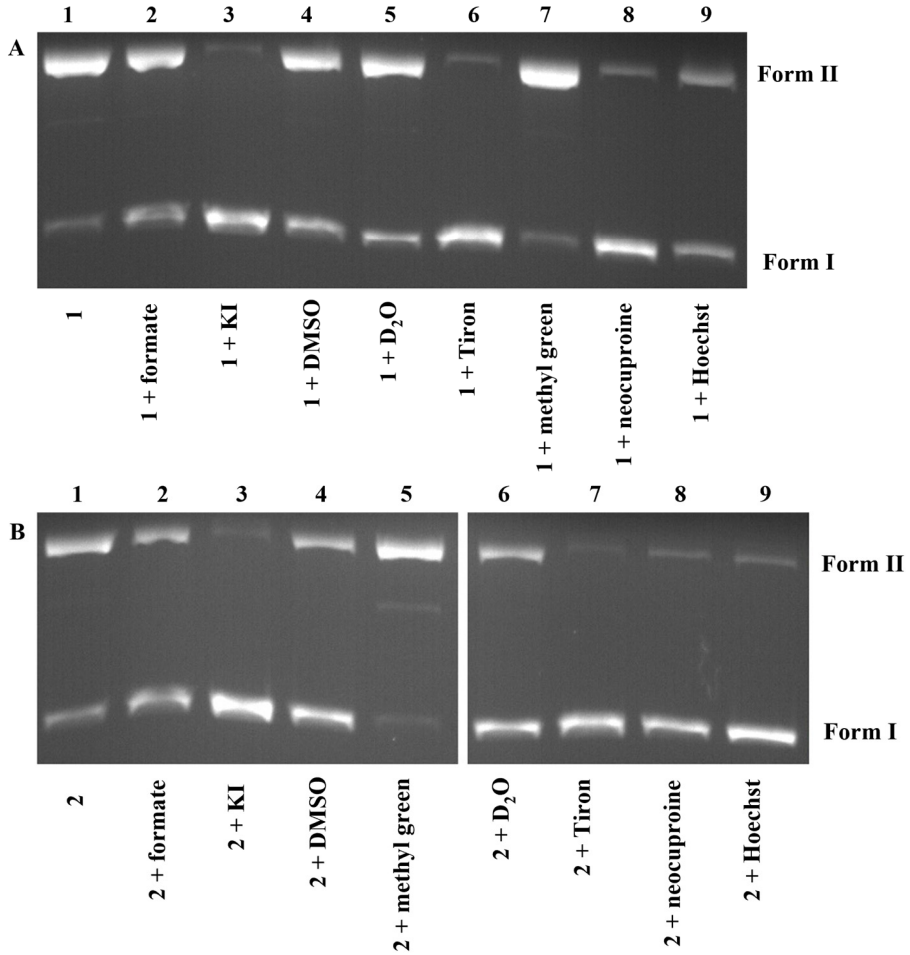

Figure 6. Agarose gel electrophoresis of pUC18 DNA treated with complexes **1** (**A**) and **2** (**B**) and ascorbate, in the presence of potential inhibitors: Lanes 2–9; complexes without inhibitors: Lane 1.

The results described above allowed us to propose a mechanism through which complexes **1** and **2** mediated nucleic acid damage in the presence of ascorbate as an activating agent. Thus, three major steps were identified as being part of the pathway, followed by the complexes that cause DNA damage:

1. An efficient interaction between the nucleic acid and the metal complex is required in order to bring the compound close to the DNA double helix. The results derived from the DNA-binding studies and from the electrophoresis show that for complexes **1** and **2,** an interaction through the DNA minor groove may be proposed.
2. The presence of ascorbate causes the reduction in Cu(II) into Cu(I), and, as a consequence, a redox cycle is initiated, generating ROS responsible for DNA damage.
3. Several ROSs are generated in a cascade of redox processes involving the Cu(I) ion, the reducing agent, and molecular oxygen. Cu(I) is reoxidized into Cu(II) as the reaction takes place in aerobic conditions. The superoxide radical formed in the same reaction undergoes a dismutation process, generating molecular oxygen and hydrogen peroxide, allowing the further formation of hydroxyl radicals, most likely through a Fenton mechanism (Figure 7). The reactive oxygen species formed ultimately caused DNA damage.

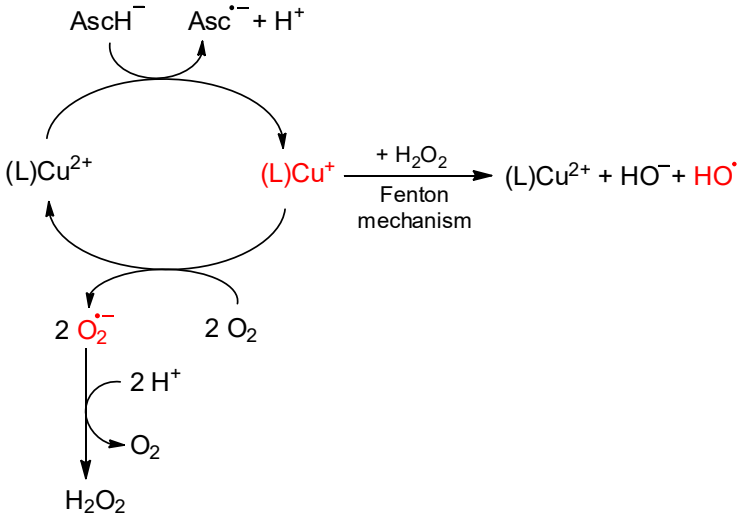

Figure 7. Proposed mechanism for the oxidative DNA cleavage mediated by complexes **1** and **2** in the presence of ascorbate. $AscH^-$: ascorbate anion, $Asc^{\bullet-}$: ascorbyl radical.

2.5. BSA-Binding Studies

The interaction of complexes **1**–**4** with BSA was evaluated by measuring the fluorescence quenching of the protein in the presence of increasing complex concentrations. The intrinsic fluorescence of BSA mainly arose from its two tryptophan residues: Trp-134, located on the surface of sub-domain IB, and Trp-212, located in a hydrophobic binding pocket in sub-domain IIA. A decrease in emission intensity might have been caused by a variety of interactions between the protein and small molecules, such as excited-state reactions, molecular rearrangements, energy transfer, and molecular collisions [56,57].

Fluorescence quenching may occur through different processes and is usually described as static quenching (when a non-fluorescent ground-state complex is formed between the fluorophore and the quencher) and dynamic quenching (when a collisional process is involved, consisting of an interaction taking place during the transient existence of the excited state). In many cases, a simultaneous static and dynamic quenching is described [56].

As shown in Figure 8, the addition of the metal complexes resulted in a concentration-dependent quenching of the intrinsic fluorescence of BSA.

In order to avoid a wrong estimation of the binding parameters, it was important verify whether the inner filter effects were significant or not. The extent of the inner filter effect was estimated with Equation (2) [54]:

$$I_{corr} = I_{meas} \times 10^{[(\varepsilon\lambda ex)cd)]/2} \times 10^{[(\varepsilon\lambda em)cd]/2} \quad (2)$$

where I_{corr} was the corrected intensity, I_{meas} was the measured intensity; c was the concentration of the quencher, d was the cuvette length (1 cm), and ελex and ελem were the ε of the quencher at the excitation and the emission wavelength, calculated from the UV-vis spectra of the complexes in a cacodylate buffer with 1% DMF (Figure S5). For our compounds, the inner-filter effect was not significant and did not affect the measurements.

Regarding the degree of the fluorescence quenching of BSA, the complexes behaved in a similar manner, causing a decrease in emission intensity of about 28%, without any significant shift in the emission maximum, which may have been a consequence of microenvironment changes around the tryptophan residues and/or the unfolding of the protein [57].

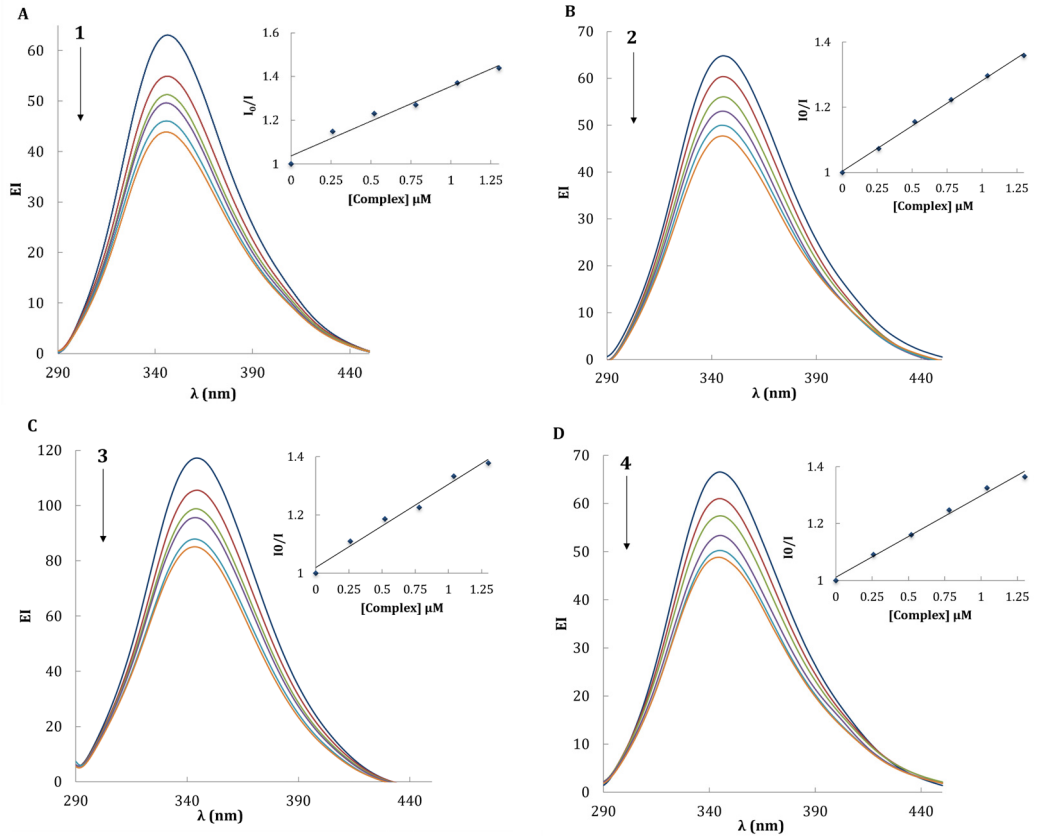

Figure 8. Emission spectra of BSA in the absence and in the presence of increasing concentrations of **1** (**A**), **2** (**B**), **3** (**C**), **4** (**D**). The arrows indicate the changes in the emission intensity at increasing complex concentrations. Inset: Stern–Volmer and Scatchard plots.

The experimental results were analyzed using the Stern–Volmer equation describing fluorescence quenching:

$$I_0/I = 1 + K_{SV}[Q] = 1 + k_q\tau_0[Q] \quad (3)$$

where I_0 and I were the fluorescence intensities of BSA in the absence and in the presence of the quencher, respectively, K_{SV} was the Stern–Volmer quenching constant, [Q] was the concentration of the quencher, k_q was the biomolecular quenching rate constant, and τ_0 was the average lifetime of the fluorophore in the absence of the quencher (10^{-8} s for BSA) [58].

A fluorescence quenching of BSA that was in good agreement with the Stern–Volmer equation was observed for all complexes, indicating that a single quenching mechanism was involved, either static or dynamic [29,47]. The K_{SV} values (Table 5) were in the order of magnitude of 10^5 M^{-1} and were similar to previously reported transition metal complexes [29,35,59]. Moreover, the biomolecular quenching constant (k_q) values calculated were of the order of magnitude of 10^{13} $M^{-1}s^{-1}$, 1000-fold higher than the maximum value for diffusion-controlled quenching (2×10^{10} $M^{-1}s^{-1}$) [58], suggesting that the probable quenching mechanism was not initiated by a dynamic process but by a static one [58,60] as a result of the formation of a ground-state non-fluorescent complex. The equilibrium between free and bound molecules, when small compounds bind independently to a set of equivalent sites on a molecule, is described by the Scatchard equation [29]:

$$\log[(I_0 - I)/I] = \log[K_b] + n \log[Q] \quad (4)$$

where I_0 and I were the fluorescence intensities of the protein in the absence and in the presence of the quencher, respectively, [Q] was the concentration of the quencher, K_b was the binding constant, and n was the number of binding sites.

Table 5. Parameters characterizing the interaction of complexes **1**–**4** with BSA.

Complex	% Hypochromism	K_{SV} (M^{-1}) × 10^5	k_q ($M^{-1}s^{-1}$) × 10^{13}	K_b (M^{-1})	n
1	30.5	3.18	3.18	3.08×10^3	0.65
2	26.4	2.78	2.78	2.33×10^5	0.98
3	27.4	2.85	2.85	1.24×10^4	0.76
4	26.7	2.87	2.87	6.79×10^4	0.89

Plots of log[(I_0 − I)/I] vs. log[Complex] are shown in Figure S4. The data for all complexes presented a linear pattern with K_b values, falling in the range of order of magnitude of 10^3–10^5 M^{-1} (Table 5). The obtained values for K_b indicated that complexes **2**–**4** had a relatively high affinity for BSA (10^4–10^5 M^{-1}) and were within what is considered to be the optimum range for the binding constant of a compound to serum albumins (10^4–10^6 M^{-1}) [61]. Generally, the binding constant of a compound to serum albumins should be high enough to guarantee that a significant quantity is transported but, at the same time, low enough so that the compound may be released once its target is reached. Complex **1** seemed to possess poor binding properties, considering its K_b value of approximately 10^3 M^{-1}. Apart from complex **1**, the number of binding sites (n) for the complexes was approximately one, suggesting that there was one independent class of binding sites to BSA for them. The values obtained for K_b and n were similar to those previously reported for transition metal complexes containing aromatic structures [29,35].

UV-Vis spectroscopy is a very useful tool in evaluating drug–protein interactions, providing information regarding the conformational changes suffered by the protein. In the case of dynamic quenching, no changes were observed in the absorption spectrum of BSA as a result of the interaction since the only one affected was the excited state of the fluorophore, but when a ground-state complex was formed, changes often occurred in the absorption spectrum of the protein. With the aim of validating the interaction mechanism of the metal complexes with BSA, we compared the UV-Vis spectrum of the protein with the one obtained upon a complex addition. After subtracting the absorption spectrum of the complex from that corresponding to the complex-BSA system, a hyperchromism was observed for all four coordination compounds, with no shift in the absorption wavelength, confirming a static quenching mechanism that resulted in protein conformational changes [62–64]. The increment in absorption may have been due to additional exposure of the aromatic amino acid residues as a consequence of protein unfolding, sustaining the findings brought forth by the fluorescence spectroscopy study [57].

2.6. Antitumor Activity

As complexes **1** and **2** showed the ability to cleave DNA, they were the ones chosen for further evaluation of their antitumor potential on the cancerous A549 cell line in parallel with normal human fibroblasts (BJ cell line). Due to the limited solubility in the cellular media, complex **1** was evaluated up to a concentration of 50 μM, while concentrations up to 100 μM were assayed for complex **2**. Both complexes displayed a significant cytotoxic effect, starting with the lowest tested dose of 10 μM for **1** and 20 μM for **2** (Figure 9). The toxicity observed was dose-dependent for both complexes in both cell types, with a slightly higher cytotoxicity being observed in the case of the cancerous phenotype (Figure 9, Table 6). In comparison with **2**, compound **1** displayed a higher cytotoxicity, having IC_{50} values at approximately half the concentration of **1** (Table 6). Besides being dose-dependent, the cytotoxicity observed in the case of A549 cells was also time-dependent, with a higher cytotoxicity being observed after an exposure of 48 h. Interestingly, in the case of BJ cells, at intermediary doses (10–25 and 20–50 μM for **1** and **2**, respectively), a higher viability was observed at 48 h than at 24 h of exposure (Figure 9). This effect could be the result of cellular resilience, the normal cells adapting to the presence of the complexes, and thus inducing a recovery of the viability [65]. In parallel with the complexes, the cellular viability was also

evaluated for the ligand (HQSMP) and the Cu(II) ions at equivalent doses to those assayed for the complexes, with no cytotoxicity observed.

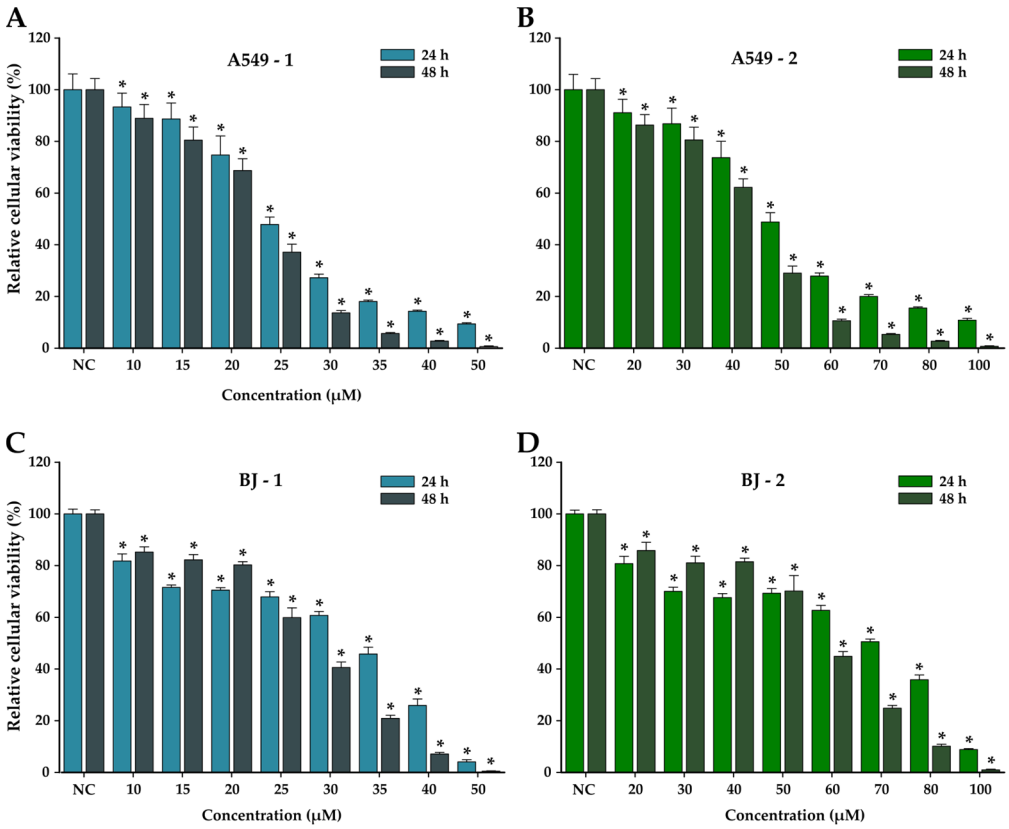

Figure 9. Cytotoxic effect of **1** (**A**,**C**) and **2** (**B**,**D**) after 24 h and 48 h of A549 (**A**,**B**) and BJ (**C**,**D**) cells. The results are expressed as relative means ± standard deviations (six technical replicates for each of the three biological replicates). Viability data were expressed as relative values where the negative control (DMSO 0.2%) is 100%. Asterisks (*) indicate significant differences ($p < 0.05$) compared to the negative control (NC).

Table 6. IC_{50} values (μM) with standard deviation after exposure of human lung adenocarcinoma (A549), and human normal foreskin fibroblasts (BJ) to complexes **1** and **2** for 24 h and 48 h.

Complex	IC50 (μM)			
	24 h		48 h	
	A549	BJ	A549	BJ
1	24.1 ± 0.4	31.6 ± 1.1	23.3 ± 0.3	29.37 ± 0.7
2	48.2 ± 0.9	66.2 ± 2.5	44.1 ± 0.7	61.35 ± 1.2

2.7. ROS Production in A549 Cells

The ability of complexes **1** and **2** to generate ROS in cellular systems was evaluated by the DCFH-DA assay on the A549 cells. After cellular internalization, the non-fluorescent DCFH-DA probe was hydrolyzed by cytoplasmatic esterases to dichlorodihydrofluorescein (DCFH), which remained sequestrated inside the cellular compartment. In the presence of an intracellular ROS, DCFH was oxidized to dichlorofluorescein, a fluorescent compound that was directly proportional to the ROS concentration. Both complexes induced the generation of ROS in a dose-dependent manner, with statistical significance being reached from the lowest exposure dose of 10 μM in the case of both complexes (Figure 10). At the highest tested dose, the level of the ROS was approximately 34 and 28 times higher for **1** and **2**, with complex **1** displaying a higher ability to generate ROS. In comparison

with the positive control (H_2O_2), where an approximately 10-fold increase in the ROS was observed for an exposure dose of 20 mM, both complexes displayed improved capabilities of generating ROS, with the concentrations needed to induce a 10-fold increase being approximately 1000 lower than the one observed in the case of the positive control (Figure S6). These results are congruent with the ones obtained in the viability assay, with complex **1** displaying a higher cytotoxicity and a higher capability to induce ROS formation.

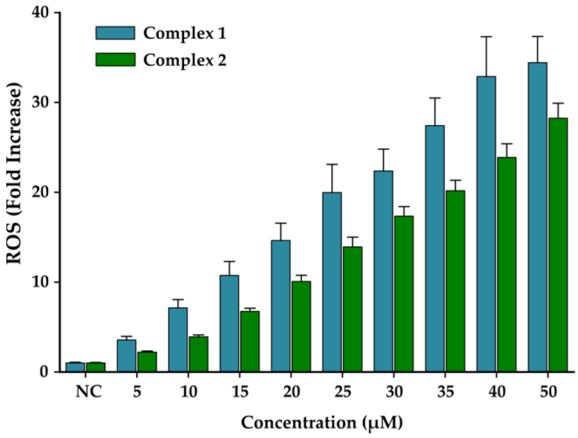

Figure 10. Induction of ROS in A549 cells after 2 h of incubation with complexes **1** and **2**. The results are expressed as the fold increase in cell fluorescence compared to the negative control (NC). The results are expressed as relative means ± standard deviations (six technical replicates for each of the three biological replicates).

3. Experimental Section

3.1. Materials and Methods

All reagents and solvents were commercially available and were used without further purification. Elemental analyses were performed on a Carlo Erba AAS instrument. NMR spectra (^{1}H, ^{13}C, HSQC, and COSY, Cornaredo, Italy) were recorded on an Advancer DRX 500 Bruker instrument in d_6-DMSO (Bruker, Madison, WI, USA). Chemical shifts are reported relative to the residual d_6-DMSO (δ_H 2.50 ppm and δ_C 39.43 ppm) [66]. IR spectra for HQSMP and complexes **2**, **3,** and **4** were recorded with a Thermo Scientific Nicolet iS10 ATR-FTIR in the range 4000–650 cm^{-1} using the Smart iTR ATR accessory (Thermo Scientific, Waltham, MA, USA). The IR spectrum for complex **one** was recorded with a Jasco FT-IR 4100 ATR FT-IR in the range 4000–550 cm^{-1} (Jasco, Tokyo Japan), and the scans were analyzed using the Jasco Manager 2.0 software. Electrospray ionization mass spectra (positive mode) analyses were performed on a Bruker Esquire 3000 plus Ion Trap Spectrometer coupled with an Agilent 1100 Chemstation LC-MS system (Agilent, Santa Clara, CA, USA). Diffuse reflectance electronic spectra were recorded on a Jasco V-550 spectrophotometer in the range of 200–800 nm. UV-Vis spectra in a solution were recorded using an Agilent 8453 spectrophotometer in the range 190–1100 nm.

3.2. Synthesis

Synthesis of HQSMP

The sulfonamide (HQSMP) ligand was obtained following the same procedure that was used for the previously reported HQSEP [29]. A total of 8.8 mmol (2 g) of solid quinoline-8-sulfonyl chloride was added to a solution containing 8.8 mmol (0.95 g) of pyridin-2-ylmethanamine in 6 mL of pyridine. The resulting suspension was stirred at 0 °C for 1 h and at room temperature for another 2 h 30 min. Then, 50 mL of cold water was added, and the reaction mixture was stirred for another 2 h in an ice bath. A solid was obtained that was filtered and recrystallized using 50 mL of ethanol at 40 °C.

Data for N-(pyridin-2-ylmethyl)quinoline-8-sulfonamide (HQSMP): Yield 1.03 g, 23%. Anal. for $C_{15}H_{13}N_3O_2S$ (MW= 299.35): calculated (found): C 60.18 (59.85); H 4.37 (4.40);

N 14.03 (14.01); S 10.71 (10.74). ^{1}H NMR (300 MHz) (d_6-DMSO, δ/ppm): 9.05 [dd, 1H, J = 4.1 Hz, J = 1.7 Hz, quinoline]; 8.50 [dd, 1H, J = 8.2 Hz, J = 1.8 Hz, quinoline]; 8.28 [dd, 1H, J = 7.6 Hz, J = 1.7 Hz, quinoline]; 8.22 [m, 2H, quinoline, pyridine]; 7.81 [t, 1H, J = 6.2 Hz, NH]; 7.70 [m, 2H, quinoline]; 7.51 [dt, 1H, J = 8.4 Hz, J = 1.7 Hz, pyridine]; 7.22 [d, 1H, J = 7.9 Hz, pyridine]; 7.07 [m, 1H, pyridine]; 4.20 [d, 2H, J = 6.3 Hz, CH_2]. ^{13}C NMR (300 MHz) (d_6-DMSO, δ/ppm): 122.6, 126.0, 128.8, 131.0, 134.0, 136.7, 137.4, 143.0, 151.7 (C quinoline); 122.0, 122.9, 136.7, 148.7, 156.9 (C pyridine); 48.6 (CH_2). IR (ν_{max}/cm^{-1}): 3188 ν(N-H); 1324 $\nu_{asym}(SO_2)$; 1165, 1147 (d) $\nu_{sym}(SO_2)$; 1041 ν(S-N). ESI$^+$ (DMF): m/z^+ 300.00 $[HQSMP + H]^+$.

Synthesis of $[Cu_2(QSMP)_2SO_4]\cdot 2H_2O$ (**1**)

A total of 0.5 mmol (124.8 mg) of solid $CuSO_4\cdot 5H_2O$ was added to a solution containing 0.5 mmol (149.6 mg) of HQSMP in 30 mL of methanol. The mixture was stirred at room temperature for 1 h. The resulting dark-blue precipitate was removed, and after approximately four days, dark-blue prismatic crystals formed in the solution but were of insufficient quality for X-ray diffraction.

Data for $[Cu_2(QSMP)_2SO_4]\cdot 2H_2O$ (**1**): Yield 94.2 mg, 22%. Anal. for $C_{30}H_{28}CuN_6O_{10}S_3$ (MW = 855.8): calculated (found): C 42.10 (42.20); H 3.27 (3.14); N 9.82 (9.72); S 11.20 (10.91). IR (ν_{max}/cm^{-1}): 1289 $\nu_{asym}(SO_2)$, 1125, 1102 (d) $\nu_{sym}(SO_2)$**;** 963 ν(S-N); 1055, 1024, 997, 608 $\nu(SO_4)$. ESI$^+$ (DMF): m/z^+ 360.9 $[Cu(QSMP)]^+$; 436.0 $[Cu(QSMP) + DMF]^+$; 821.0 $[Cu_2(QSMP)_2SO_4 + H]^+$. Solid UV-Vis (λ_{max}/nm): 325, 730. UV-Vis (DMF) (λ_{max}/nm): 316sh, 709 (ε = 229.71 $cm^{-1}M^{-1}$).

Synthesis of $[Cu(QSMP)Cl]_n$ (**2**)

To a solution of 0.5 mmol (149.6 mg) HQSMP in 30 mL of methanol, 0.5 mmol (85.2 mg) of solid $CuCl_2\cdot 2H_2O$ was added. The mixture was stirred at room temperature for 1 h. The resulting light-blue precipitate was removed, and after approximately five days, needle-shaped turquoise-blue crystals, suitable for X-ray diffraction, formed in the filtrate. Crystals were isolated by filtration, washed with methanol, and dried under a vacuum.

Data for $[Cu(QSMP)Cl]_n$ (**2**): Yield 59.6 mg, 30%. Anal. for $C_{15}H_{12}CuN_3O_2SCl$ (MW = 397.33): calculated (found): C 45.33 (45.32); H 3.02 (2.94); N 10.57 (10.60); S 8.06 (8.01). IR (ν_{max}/cm^{-1}): 1244 $\nu_{asym}(SO_2)$, 1090 $\nu_{sym}(SO_2)$; 996 ν(S-N). ESI$^+$ (DMF): m/z^+ 360.9 $[Cu(QSMP)]^+$; 398.7 $[Cu(QSMP)Cl + H^+]^+$. Solid UV-Vis (λ_{max}/nm): 380sh, 735. UV-Vis (DMF) (λ_{max}/nm): 408, 723 (ε = 126.21 $cm^{-1}M^{-1}$).

Synthesis of $[Cu(QSMP)(C_6H_5COO)]$ (**3**)

A total of 0.25 mmol (34.3 mg) of solid $CuF_2\cdot 2H_2O$ was added to a solution of 0.25 mmol (74.8 mg) of HQSMP in 10 mL of methanol. After the complete dissolution of the copper salt, 0.25 mmol (34.7 mg) of solid $C_6H_5COONH_4$ was added to the initial mixture, and the brown precipitate formed was removed. By slow evaporation of the solvent, after approximately three days, dark-blue plate crystals, suitable for X-ray diffraction, formed in the solution. Crystals were isolated by means of filtration, washed with methanol, and dried under a vacuum.

Data for $[Cu(QSMP)(C_6H_5COO)]$ (**3**): Yield 50.7 mg, 42%. Anal. for $C_{22}H_{17}CuN_3O_4S$ (MW = 482.97): calculated (found): C 54.70 (54.89); H 3.51 (3.50); N 8.70 (8.74); S 6.63 (6.60). IR (ν_{max}/cm^{-1}): 1296 $\nu_{asym}(SO_2)$, 1140 $\nu_{sym}(SO_2)$**;** 936 ν(S-N); 1563 $\nu_{asym}(COO)$; 1441 $\nu_{sym}(COO)$. ESI$^+$ (DMF): m/z^+ 360.9 $[Cu(QSMP)]^+$; 482.7 $[Cu(QSMP)C_6H_5COO + H^+]^+$; 503.6 $[Cu(QSMP)C_6H_5COO + DMF + H^+]^+$. Solid UV-Vis ($\lambda_{max}$/nm): 395 sh, 700. UV-Vis (DMF) (λ_{max}/nm): 377 sh, 685 (ε = 137.92 $cm^{-1}M^{-1}$).

Synthesis of $[Ni(QSMP)(C_6H_5COO)(CH_3OH)][Ni(QSMP)(CH_3COO)(CH_3OH)]$ (**4**)

A total of 1 mmol (248.8 mg) of solid $Ni(CH_3COO)_2\cdot 4H_2O$ was added to a solution containing 0.5 mmol (149.6 mg) of HQSMP in 15 mL of methanol. After the complete dissolution of the nickel salt, 0.5 mmol (69.4 mg) of solid $C_6H_5COONH_4$ was added. The resulting dark green solution was stirred at room temperature for 1 h. Within 24 h, well-formed blue plate crystals, suitable for X-ray diffraction, formed in the filtrate.

Data for [Ni(QSMP)(C_6H_5COO)(CH_3OH)][Ni(QSMP)(CH_3COO)(CH_3OH)] (**4**): Yield 95.8 mg, 25%. Anal. for $C_{41}H_{40}Ni_2N_6O_{10}S_2$ (MW = 958.33): calculated(found): C 51.38(51.64); H 4.10(4.11); N 8.77(8.50); S 6.69(6.40). IR (ν_{max}/cm^{-1}): 1255 $\nu_{asym}(SO_2)$, 1132 $\nu_{sym}(SO_2)$; 1020 ν(S-N); 1519 $\nu_{asym}(COO)$; 1418 $\nu_{sym}(COO)$; 3262 ν(O-H). ESI^+ (DMF): m/z^+ 356.0 $[Ni(QSMP)]^+$; 489.3 $[Ni(QSMP)(CH_3COO)(CH_3OH) + K^+]^+$; 510.1 $[Ni(QSMP)(C_6H_5COO)(CH_3OH) + H^+]^+$; 655.1 $[Ni(QSMP)_2 + H]^+$. Solid UV-Vis (λ_{max}/nm): 330, 640. UV-Vis (DMF) (λ_{max}/nm): 318sh, 630 (ε = 34.56 $cm^{-1}M^{-1}$).

3.3. X-ray Data Collection and Structure Refinement

A summary of the crystal data, experimental details, and refinement results is listed in Table 7.

Table 7. Crystal data and structure refinement for complexes **2**–**4**.

	2	**3**	**4**
Empirical formula	$C_{15}H_{12}CuN_3O_2SCl$	$C_{22}H_{17}CuN_3O_4S$	$C_{41}H_{40}Ni_2N_6O_{10}S_2$
Formula weight	397.33	482.98	958.33
Temperature (K)	100 (2) K	100 (2) K	100 (2) K
Wavelength (Å)	0.71073	0.71073	0.71069
Crystal system, space group	Monoclinic, $P2_1/c$	Monoclinic, $P2_1/c$	Monoclinic, $P2_1/n$
a [Å]	11.7685(8)	8.2565(4)	8.992(5)
b [Å]	13.7587(9)	8.8840(4)	21.456(5)
c [Å]	10.0538(6)	27.3508(14)	10.444(5)
α [°]	90	90	90
β [°]	112.698(3)	97.162(2)	93.809(5)
γ [°]	90	90	90
Volume [$Å^3$]	1501.82(17)	1990.55(17)	2010.5(15)
Z, calculated density [mg/m^3]	4, 1.757	4, 1.612	2, 1.583
Absorption coefficient [mm^{-1}]	1.783	1.239	1.108
F(000)	804	988	992
Crystal size [mm]	0.32 × 0.08 × 0.04	0.230 × 0.170 × 0.020	0.24 × 0.13 × 0.10
θ range for data collection [°]	1.88 to 30.51	1.501 to 26.371	2.17 to 27.10
Limiting indices	$-16 \leq h \leq 15$ $0 \leq k \leq 19$ $0 \leq l \leq 14$	$-10 \leq h \leq 10$ $0 \leq k \leq 11$ $0 \leq l \leq 34$	$-11 \leq h \leq 11$ $0 \leq k \leq 27$ $0 \leq l \leq 13$
Reflections collected/unique	62,895/4589 [R(int) = 0.0543]	19,079/4068 [R(int) = 0.0466]	31,379/4437 [R(int) = 0.0599]
Completeness to θ [%]	10 θ = 30.51	100 θ = 25.242	99.9 θ = 27.10
Absorption correction	Semi-empirical from equivalents	Semi-empirical from equivalents	Semi-empirical from equivalents
Max./min. transmission	0.9321/0.5992	1.000/0.900	0.8972/0.7768
Refinement method	Full-matrix least-squares on F^2	Full-matrix least-squares on F^2	Full-matrix least-squares on F^2
Data/restraints/parameters	4589/0/208	4068/0/280	4437/12/307
Goodness-of-fit on F^2	1.045	1.034	1.222
Final *R* indices	R1 = 0.0258	R1 = 0.0325	R1 = 0.0455
[$I > 2\sigma(I)$]	wR2 = 0.0593	wR2 = 0.0746	wR2 = 0.0951
R indices	R1 = 0.0370	R1 = 0.0450	R1 = 0.0532
(all data)	wR2 = 0.0640	wR2 = 0.0804	wR2 = 0.0976
Largest diff. peak/hole [$e \cdot Å^3$]	0.491/−0.462	0.469/−0.437	0.389/−0.403
CCDC	2349438	2349437	2349439

Crystal data were collected at 100(2) K using a Bruker KappaAPEXII (**2** and **3**), and a Bruker SMART CCD 1000 (**4**) diffractometer from crystals mounted on glass fibers. Graphite monochromatic MoK(alpha) radiation was used throughout. The data were processed with APEX2 [67] (**2** and **3**) and SAINT [68] (**4**) and corrected for absorption using SADABS [69]. The structures were solved by direct methods and refined by full-matrix least-squares

techniques against F^2 [70]. Positional and anisotropic atomic displacement parameters were refined for all nonhydrogen atoms. Hydrogen atoms were included in geometrically idealized positions employing appropriate riding models with isotropic displacement parameters constrained to 1.2 U~(eq) of their carrier atoms. The criteria for a satisfactory complete analysis were that the ratios of the "rms" shifted to a standard deviation of less than 0.001, and there were no significant features in the final difference maps. Atomic scattering factors were taken from "International Tables for Crystallography" [71]. Molecular graphics were generated with DIAMOND [59]. For complex **4**, C atoms of the methyl group and phenyl ring of acetate and benzoate ligands, respectively, were refined with an occupancy of 0.5. Final refinement [70] included the displacement coefficient restraints of ISOR of 0.005 for C30 and C32 to prevent the atoms from becoming "non-positive definite". CCDC 2349438 (for **2**), CCDC 2349437 (for **3**), and CCDC 2349439 (for **4**) contain the supplementary crystallographic data for this paper. The data can be obtained free of charge from the Cambridge Crystallographic Data Centre.

3.4. DNA-Binding Studies

Calf thymus DNA (CT-DNA, type XV) was used in all experiments regarding the ability of the complexes to interact with DNA. The concentration of CT–DNA was determined from its absorption intensity at 260 nm with a molar extinction coefficient of 6600 M^{-1} cm^{-1} [50]. The UV absorbance at 260 nm and 280 nm gave a ratio of 1.8–1.9, indicating that the DNA was sufficiently free of the protein. Stock solutions of the complexes were prepared in DMF. Final samples contained a maximum of 5% DMF for all DNA-binding experiments.

DNA thermal denaturation experiments were carried out by recording the absorbance spectra at 260 nm of 100 μM CT-DNA in 1 mM phosphate buffer, 2 mM NaCl, pH = 7.2, in the temperature range of 25–75 °C. Experiments were performed in the absence and in the presence of the metal complexes in a [DNA]:[Complex] = 2:1 or 4:1 ratio, with final samples containing 5% DMF for complexes **1**–**3** and 1% DMF for complex **4**. The spectra were recorded using an Agilent 8453 UV-Vis spectrophotometer equipped with a Peltier temperature-controlled sample cell and driver (Agilent 89090A). The samples were stirred continuously during the experiment, and the temperature was set at 1 °C/min. The DNA melting point was obtained with the first derivative by applying the Savitsky–Golay algorithm.

The fluorescence spectra were recorded using a JASCO FP-6200 spectrofluorimeter at room temperature. Complex solutions were added to samples containing 50 μM CT-DNA and 50 μM ethidium bromide (EB) in 0.1 M cacodylate buffer, pH = 6.0. Complex concentrations ranged from 0 to 80 μM, with a maximum of 5% DMF in the final sample. The excitation wavelength used was 500 nm, and the emission was recorded between 530 nm and 680 nm.

3.5. DNA Cleavage and Mechanistic Studies

All experiments consisted of subjecting the samples to horizontal electrophoresis on a 0.8% agarose gel in 0.5× TBE buffer (0.045 M Tris, 0.045 M boric acid, and 1 mM EDTA) stained with EB (2 μL/100 mL, stock solution 10 mg/mL) as support. The electrophoretic separation was performed at 120 V for 2 h, and the gel was photographed under UV light using a Uvitec Cambridge UVIdoc HD2/20MX camera.

The nuclease activity of complexes **1** and **2** was studied in the presence of ascorbate as a reducing agent, with all samples containing 5% DMF. Reactions were performed in cacodylate buffer (pH = 6.0), with pUC18 supercoiled DNA (0.5 μg/μL, 2686 base pairs, molecular weight 1.74×10^6 Da, stored in 10 mM Tris-HCl and 1 mM EDTA buffer, pH = 7.6, Thermo Scientific) and complex solutions at increasing concentrations to obtain final complex concentrations in the range 10–25 μM. Ascorbate was used at the same concentration as the complex. The mixtures were incubated at 37 °C for an hour, after which loading buffer (0.25% bromophenol blue, 0.25% xylene cyanol, 30% glycerol) was added.

In order to identify the reactive oxygen species (ROS) involved in DNA scission and the possible complex-DNA interaction modes, various ROS intermediate scavengers were added to the reaction mixtures: sodium formate (0.4 M), potassium iodide (0.4 M), DMSO (0.4 M) and 4,5-dihydroxy-1,3-benzenedisulfonic acid disodium salt monohydrate (Tiron) (10 mM). In addition, a Cu(I) chelating agent, neocuproine (100 μM), and groove binders Hoechst 33258 (8 μM) and methyl green (3 μM) were assayed. For one of the samples, D_2O was used to dilute the final volume.

3.6. BSA-Binding Studies

The affinity of the complexes towards BSA and the type of interaction established with the protein were evaluated by means of fluorescence and UV-Vis spectroscopy. Quantitative analyses of the interaction between the complexes and BSA were performed using fluorimetric titration. The spectra were recorded using a JASCO FP-6200 spectrofluorimeter at room temperature. A stock solution of BSA (5.0×10^{-4} M) was prepared in 0.1 M cacodylate buffer (pH = 6.0). The BSA solution was stored at 0–4 °C in the dark and used within a maximum of 48 h. To samples containing 1.3 μM BSA in 0.1 M cacodylate buffer (pH = 6.0), complex solutions were added in order to obtain [Complex]:[BSA] ratios ranging from 0 to 1, with a maximum of 2.5% DMF. After each complex addition, the mixture was kept in the dark for 20 min at room temperature. The excitation wavelength used was 280 nm, and the emission was recorded between 290 nm and 450 nm. The UV-Vis spectra were recorded using an Agilent 8453 UV-Vis spectrophotometer, using a BSA solution (3.3×10^{-5} M) in cacodylate buffer (pH = 6). The changes to the BSA spectrum were monitored, specifically the absorption around 280 nm, upon the addition of complex solutions in a [BSA]: [Complex] = 1:1 ratio, with final samples containing 1% DMF.

3.7. Biological Activities on Cell Lines

3.7.1. Cell Culture

For the evaluation of the antitumor and pro-oxidant properties of the complexes, normal human foreskin fibroblasts (BJ) and the A549 cancerous cells (lung adenocarcinoma) purchased from ATCC (Manassas, VA, USA) were used. The normal cell phenotype was maintained in DMEM (Dulbecco's modified Eagle's medium) with low glucose (1 g/L), while the cancerous cells were cultured in DMEM with high glucose (5 g/L). Both media were supplemented with 10% FBS (fetal bovine serum). Cells were kept at 37 °C in a humidified incubator with 5% CO_2 addition. Cellular media were replaced every other day, and the cells were either subcultured or used for experimentation at a confluency of 70–80%.

3.7.2. Antitumor Activity

Cancerous (A549) and normal (BJ) cells were seeded in 96 well plates and left to attach to the substrate for 24 h. Dead and unattached cells were washed with PBS while the remaining viable cells were further exposed for 24 h/48 h at concentrations ranging from 10 to 50 μM for complex **one** and 20 to 100 μM for complex **2**. After the exposure, the cellular medium was removed, the cells were washed with PBS, and the viability was measured using the Alamar Blue (AB) assay. Briefly, the cells were exposed to a 200 μM resazurin solution for 4 h, and the fluorescence was measured at $\lambda_{excitation}$ = 530/25 and $\lambda_{emission}$ = 590/35, using Synergy 2 Multi-Mode Microplate Reader. The experiment was conducted using three biological replicates, each one including 6 technical replicates. Cells exposed to the vehicle (culture medium containing 0.2% DMSO) were used as a negative control. The results were presented as relative values compared to the negative control (100%). For a more straightforward interpretation of the results, IC_{50} values were calculated from the dose-effect curves obtained by fitting the experimental data with a 4-parameter logistic curve in SigmaPlot 11.0 software.

3.7.3. Dichloro-Fluorescein Diacetate (DCFH-DA) Assay

The ability of the complexes to generate a reactive oxygen species (ROS) in the cellular milieu was evaluated on the A549 cancerous cells using the 2,7 dichloro-fluorescein diacetate (DCFH-DA) dye. Briefly, cells were loaded for 2 h with 50 μM DCFH-DA dye dissolved in Hanks' balanced salt solution (HBSS) and washed 2 × 2X with PBS to remove extracellular dye. Cells were further incubated with the two complexes at concentrations ranging from 5 to 50 μM for another 2 h, and the fluorescence was measured using a Synergy 2 multi-mode microplate reader at $\lambda_{excitation}$ = 485/20 and $\lambda_{emission}$ = 528/20. Three biological replicates, each one including 6 technical replicates, were performed, and the results were expressed as relative values compared to the negative control.

3.8. Statistical Analysis

Experimental data are presented as mean values ± standard deviations (SD) of three biological replicates. Data were statistically analyzed using One-Way Analysis of Variance (ANOVA) with a Holm–Sidak post hoc test. Graphical representation and data analysis were performed using the SigmaPlot 11 software (Systat, Software Inc., Chicago, IL, USA). Results were considered statistically different if *p*-values were lower than 0.05.

4. Conclusions

New sulfonamide metal complexes containing essential transition metal ions [Cu(II) and Ni(II)] have been synthesized and thoroughly characterized. Noteworthy, in compound **2,** the sulfonamide ligand acted as a bridge, giving a polymeric structure, a coordination behavior that is unusual for quinoline sulfonamide derivatives. Moreover, their biological properties were studied, with a focus on nucleic acid and protein interactions. Both UV-Vis and fluorescent studies showed that complex **4**, containing a Ni(II) metal center, had the highest affinity towards DNA, a phenomenon that was previously reported by our group for other series of similar compounds. The DNA cleavage capabilities of complexes **1** and **2** in the presence of ascorbate were very similar, with the compounds being able to transform the nucleic acid from its supercoiled form to the open circular and linear ones at a relatively low concentration, 20 μM. By performing mechanistic studies, we concluded that the DNA damage was induced by generating superoxide and hydroxyl radicals. Moreover, we were able to propose an interaction with the DNA for complexes **1** and **2** through the DNA minor groove. The interaction of the compounds with BSA was also investigated, revealing that complex **1** had poor binding properties, whereas the binding constant for complexes **2**–**4** was within the optimum range (10^4–10^6 M^{-1}). The antitumor activity studies performed for complexes **1** and **2** revealed that they possessed significant dose- and time-dependent cytotoxic properties as a consequence of the DNA damage induced by the ROS.

The results presented in this work show that the complexes possessed interesting biological properties due to their ability to interact with biomacromolecules, namely DNA and BSA, providing valuable information that could be the basis for developing new chemotherapeutic drugs.

Supplementary Materials: The following supporting information can be downloaded at https://www.mdpi.com/article/10.3390/inorganics12060158/s1, Figure S1: IR spectra of HQSMP (A) and complexes **1** (B), **2** (C), **3** (D) and **4** (E). Figure S2: UV-Vis spectra of complexes **1** (A1, A2), **2** (B1, B2), **3** (C) and **4** (D1, D2) in DMF solution. Figure S3: DNA melting curves in the absence and in the presence of HQSMR (A) and complexes **1**, **2**, **3** (B) and **4** (C). Figure S4: BSA-binding data presented in the form of log(I_0–I/I) vs. log[complex] for complexes 1 (A), 2 (B), 3 (C) and 4 (D). Figure S5: UV spectra of complexes **1** (A1, A2), **2** (B1, B2), **3** (C) and **4** (D1, D2) in cacodylate buffer with 1% DMF. Figure S6: Induction of ROS in A549 cells after 2 h of incubation with H_2O_2.

Author Contributions: CRediT: T.L.T.: investigation, formal analysis, visualization, writing—original draft; writing—review and editing; I.F., A.-E.P., A.C. and M.E.: investigation, formal analysis, visualization; A.E.B. and L.S.O.: writing—review and editing; G.A.-P.: conceptualization, methodology, supervision, validation, writing—review and editing. All authors have read and agreed to the published version of the manuscript.

Funding: The present work benefited from financial support through project POSDRU 107/1.5/S/78702. M.E. and G.A.-P. gratefully thank the Spanish Ministerio de Ciencia e Innovación (PID2020-115294GB-I00) for financial support. M. E. thanks the Spanish Ministerio de Universidades for postdoctoral grant (MS21-140).

Data Availability Statement: The authors confirm that the data supporting the findings of this study are available within the article.

Conflicts of Interest: The authors declare no conflicts of interest.

References

1. Rosenberg, B. Some biological effects of platinum compounds. New agents for the control of tumours. *Platin. Met. Rev.* **1971**, *15*, 42–51. [CrossRef]
2. Gailer, J. Improving the safety of metal-based drugs by tuning their metabolism with chemoprotective agents. *J. Inorg. Biochem.* **2018**, *179*, 154–157. [CrossRef]
3. de Almeida, L.C.; Calil, F.A.; Machado-Neto, J.A.; Costa-Lotufo, L.V. DNA damaging agents and DNA repair: From carcinogenesis to cancer therapy. *Cancer Genet.* **2021**, *252–253*, 6–24. [CrossRef] [PubMed]
4. Paprocka, R.; Wiese-Szadkowska, M.; Janciauskiene, S.; Kosmalski, T.; Kulik, M.; Helmin-Basa, A. Latest developments in metal complexes as anticancer agents. *Coord. Chem. Rev.* **2022**, *452*, 214307. [CrossRef]
5. Andrezalova, L.; Orszaghova, Z. Covalent and noncovalent interactions of coordination compounds with DNA: An overview. *J. Inorg. Biochem.* **2021**, *225*, 111624. [CrossRef] [PubMed]
6. Topală, T.; Bodoki, A.; Oprean, L.; Oprean, R. Experimental techniques employed in the study of metal complexes-DNA-interactions. *Farmacia* **2014**, *62*, 1049–1061.
7. Barone, G.; Terenzi, A.; Lauria, A.; Almerico, A.M.; Leal, J.M.; Busto, N.; García, B. DNA-binding of nickel(II), copper(II) and zinc(II) complexes: Structure–affinity relationships. *Coord. Chem. Rev.* **2013**, *257*, 2848–2862. [CrossRef]
8. Nakamoto, K.; Tsuboi, M.; Strahan, G.D. *Drug-DNA Interactions. Structures and Spectra*; John Wiley and Sons LTD: New York, NY, USA, 2008.
9. Garcia-Gimenez, J.L.; Hernandez-Gil, J.; Martinez-Ruiz, A.; Castineiras, A.; Liu-Gonzalez, M.; Pallardo, F.V.; Borras, J.; Alzuet Pina, G. DNA binding, nuclease activity, DNA photocleavage and cytotoxic properties of Cu(II) complexes of N-substituted sulfonamides. *J. Inorg. Biochem.* **2013**, *121*, 167–178. [CrossRef]
10. Roat-Mallone, R.M. *Bioinorganic Chemistry. A Short Course*; John Wiley & Sons, Inc.: Hoboken, NJ, USA, 2002.
11. Yu, Z.; Cowan, J.A. Metal complexes promoting catalytic cleavage of nucleic acids-biochemical tools and therapeutics. *Curr. Opin. Chem. Biol.* **2018**, *43*, 37–42. [CrossRef]
12. Zhang, P.S.; Sadler, P.J. Redox-active metal complexes for anticancer therapy. *Eur. J. Inorg. Chem.* **2017**, *2017*, 1541–1548. [CrossRef]
13. Desbouis, D.; Troitsky, I.P.; Belousoff, M.J.; Spiccia, L.; Graham, B. Copper(II), zinc(II) and nickel(II) complexes as nuclease mimetics. *Coord. Chem. Rev.* **2012**, *256*, 897–937. [CrossRef]
14. Jiang, Q.X.; Xiao, N.; Shi, P.; Zhu, Y.; Guo, Z. Design of artificial metallonucleases with oxidative mechanism. *Coord. Chem. Rev.* **2007**, *251*, 1951–1972. [CrossRef]
15. Zuin Fantoni, N.; Molphy, Z.; Slator, C.; Menounou, G.; Toniolo, G.; Mitrikas, G.; McKee, V.; Chatgilialoglu, C.; Kellett, A. Polypyridyl-based copper phenanthrene complexes: A new type of stabilized artificial chemical nuclease. *Chemistry* **2019**, *25*, 221–237. [CrossRef] [PubMed]
16. Yousuf, I.; Bashir, M.; Arjmand, F.; Tabassum, S. Advancement of metal compounds as therapeutic and diagnostic metallodrugs: Current frontiers and future perspectives. *Coord. Chem. Rev.* **2021**, *445*, 214104. [CrossRef]
17. Boros, E.; Dyson, P.J.; Gasser, G. Classification of Metal-Based Drugs according to Their Mechanisms of Action. *Chem* **2020**, *6*, 41–60. [CrossRef] [PubMed]
18. Hadjiliadis, N.S.; Sletten, E. *Metal Complex-DNA Interactions*; John Wiley & Sons, Inc.: Hoboken, NJ, USA, 2009.
19. Jopp, M.B.; Becker, J.; Becker, S.; Mishka, A.; Gandin, V.; Marzano, C.; Schindler, S. Anticancer activity of a series of copper(II) complexes with tripodal ligands. *Eur. J. Med. Chem.* **2017**, *132*, 274–281. [CrossRef] [PubMed]
20. Topală, T.; Bodoki, A.; Gheorghe-Cetean, S.; Hangan, A.; Oprean, L. Sulfonamide-containing transition metal complexes with therapeutic potential. In *Sulfonamides: An Overview*; Sarkar, D., Ed.; Nova Science Publishers: Hauppauge, NY, USA, 2020.
21. Apaydın, S.; Török, M. Sulfonamide derivatives as multi-target agents for complex diseases. *Bioorg. Med. Chem. Lett.* **2019**, *29*, 2042–2050. [CrossRef] [PubMed]
22. Mondal, S.; Malakar, S. Synthesis of sulfonamide and their synthetic and therapeutic applications: Recent advances. *Tetrahedron* **2020**, *76*, 131662. [CrossRef]

23. Castaño, L.F.; Cuartas, V.; Bernal, A.; Insuasty, A.; Guzman, J.; Vidal, O.; Rubio, V.; Puerto, G.; Lukáč, P.; Vimberg, V.; et al. New chalcone-sulfonamide hybrids exhibiting anticancer and antituberculosis activity. *Eur. J. Med. Chem.* **2019**, *176*, 50–60. [CrossRef]
24. Yurttaş, L.; Çiftçi, G.A. New quinoline based sulfonamide derivatives: Cytotoxic and apoptotic activity evaluation against pancreatic cancer cells. *Anti-Cancer Agents Med. Chem.* **2018**, *18*, 1122–1130. [CrossRef]
25. Liu, Y.; Wu, Y.; Sun, l.; Gu, Y.; Hu, L. Synthesis and structure-activity relationship study of water-soluble carbazole sulfonamide derivatives as new anticancer agents. *Eur. J. Med. Chem.* **2020**, *191*, 112181. [CrossRef] [PubMed]
26. Wan, Y.; Fang, G.; Chen, H.; Deng, X.; Tang, Z. Sulfonamide derivatives as potential anti-cancer agents and their SARs elucidation. *Eur. J. Med. Chem.* **2021**, *226*, 113837. [CrossRef] [PubMed]
27. Topală, T.; Bodoki, A.E.; Hangan, A.; Gheorghe-Cetean, S.; Oprean, L. Revisiting therapeutic sulfonamides in the attempt to improve the antimicrobial properties through metal-ion coordination. *Farmacia* **2019**, *67*, 749–758. [CrossRef]
28. Peters, T.J. *All about Albumin: Biochemistry, Genetics, and Medical Applications*; Academic Press: San Diego, CA, USA, 1995.
29. Topală, T.; Pascual-Álvarez, A.; Moldes-Tolosa, M.A.; Bodoki, A.; Castiñeiras, A.; Torres, J.; Del Pozo, C.; Borrás, J.; Alzuet-Piña, G. New sulfonamide complexes with essential metal ions [Cu (II), Co (II), Ni (II) and Zn (II)]. Effect of the geometry and the metal ion on DNA binding and nuclease activity. BSA protein interaction. *J. Inorg. Biochem.* **2020**, *202*, 110823. [CrossRef] [PubMed]
30. González-Álvarez, M.; Pascual-Álvarez, A.; del Castillo Agudo, L.; Castiñeiras, A.; Liu-González, M.; Borrás, J.; Alzuet-Piña, G. Mixed-ligand copper(II)-sulfonamide complexes: Effect of the sulfonamide derivative on DNA binding, DNA cleavage, genotoxicity and anticancer activity. *J. Chem. Soc. Dalton Trans.* **2013**, *42*, 10244–10259. [CrossRef]
31. García-Giménez, J.L.; Gonzalez-Álvarez, M.; Liu-González, M.; Macias, B.; Borrás, J.; Alzuet, G. Toward the development of metal-based synthetic nucleases: DNA binding and oxidative DNA cleavage of a mixed copper(II) complex with *N*-(9*H*-purin-6-yl)benzenesulfonamide and 1,10-phenantroline. Antitumor activity in human Caco-2 cells and Jurkat T lymphocytes. Evaluation of *p53* and *Bcl-2* proteins in the apoptotic mechanism. *J. Inorg. Biochem.* **2009**, *103*, 923–934. [CrossRef] [PubMed]
32. García-Giménez, J.L.; Alzuet, G.; González-Álvarez, M.; Liu-González, M.; Castiñeiras, A.; Borrás, J. Oxidative nuclease activity of ferromagnetically coupled μ-hydroxo-μ-propionato copper(II) complexes $[Cu_3(L)_2(\mu\text{-}OH)_2(\mu\text{-propionato})_2]$ (L=N-(pyrid-2-ylmethyl)R-sulfonamidato, R=benzene, toluene, naphthalene). *J. Inorg. Biochem.* **2009**, *103*, 243–255. [CrossRef] [PubMed]
33. Bodoki, A.; Hangan, A.; Oprean, L.; Alzuet, G.; Castiñeiras, A.; Borrás, J. Oxidative DNA cleavage by copper ternary complexes of 1,10-phenanthroline and ethylenediamine-sulfonamide derivatives. *Polyhedron* **2009**, *28*, 2537–2544. [CrossRef]
34. González-Álvarez, M.; Alzuet, G.; Borrás, J.; del Castillo-Agudo, L.; Montejo-Bernardo, J.; Gutiérrez-Rodríguez, A.; García-Granda, S. Evaluation of antiproliferative activities and apoptosis induction caused by copper(II)–benzothiazolesulfonamide complexes in Jurkat T lymphocytes and Caco-2 cells. *J. Inorg. Biochem.* **2008**, *13*, 1249–1265. [CrossRef]
35. Pascual-Álvarez, A.; Topală, T.; Estevan, F.; Sanz, F.; Alzuet-Piña, G. Photoinduced and self-activated nuclease activity of copper(II) complexes with N-(quinolin-8-yl)quinolin-8-sulfonamide—DNA and bovine serum albumin binding. *Eur. J. Inorg. Chem.* **2016**, *2016*, 982–994. [CrossRef]
36. Addison, A.W.; Rao, T.N.; Reedijk, J.; van Rijn, J.; Verschoor, G.C. Synthesis, structure, and spectroscopic properties of copper(II) compounds containing nitrogen?sulphur donor ligands; the crystal and molecular structure of aqua[1,7-bis(N-methylbenzimidazol-2?-yl)-2,6-dithiaheptane]copper(II) perchlorate. *J. Chem. Soc., Dalton Trans.* **1984**, *7*, 1349–1356. [CrossRef]
37. Marlier, E.E.; Sadowsky, D.; Cramer, C.J.; McNeill, K. Metal ion size and coordination mode in complexes of a β-diketiminate ligand with pendant quinoline arms. *Inorg. Chim. Acta* **2011**, *369*, 173–179. [CrossRef]
38. Zhang, J.-A.; Pan, M.; Jiang, J.-J.; She, Z.-G.; Fan, Z.-J.; Su, C.-Y. Syntheses, crystal structures and antimicrobial activities of thioether ligands containing quinoline and pyridine terminal groups and their transition metal complexes. *Inorg. Chim. Acta* **2011**, *374*, 269–277. [CrossRef]
39. Peng, X.; Cui, G.; Li, D.; Liu, T. Synthesis, characterization, and theoretical calculations of mononuclear copper(II) benzoate complex with 2-propylimidazole, $[Cu(PIM)_2(PhCOO)_2]$. *J. Mol. Struct.* **2010**, *967*, 54–60. [CrossRef]
40. Cano, J.; De Munno, G.; Sanz, J.L.; Ruiz, R.; Faus, J.; Lloret, F.; Julve, M.; Caneschi, A. Ability of terephthalate (ta) to mediate exchange coupling in ta-bridged copper(II), nickel(II), cobalt(II) and manganese(II) dinuclear complexes. *J. Chem. Soc. Dalton Trans.* **1997**, 1915–1923. [CrossRef]
41. Krishnamoorthy, P.; Sathyadevi, P.; Cowley, A.H.; Butorac, R.R.; Dharmaraj, N. Evaluation of DNA binding, DNA cleavage, protein binding and in vitro cytotoxic activities of bivalent transition metal hydrazone complexes. *Eur. J. Med. Chem.* **2011**, *46*, 3376–3387. [CrossRef]
42. Sathyadevi, P.; Krishnamoorthy, P.; Jayanthi, E.; Butorac, R.R.; Cowley, A.H.; Dharmaraj, N. Studies on the effect of metal ions of hydrazone complexes on interaction with nucleic acids, bovine serum albumin and antioxidant properties. *Inorg. Chim. Acta* **2012**, *384*, 83–96. [CrossRef]
43. Macías, B.; García, I.; Villa, M.a.V.; Borrás, J.; Castiñeiras, A.; Sanz, F. Synthesis and characterization of sulfonamides containing 8-aminoquinoline and their Ni(II) complexes. Crystalline structures of the Ni complexes. *Polyhedron* **2002**, *21*, 1229–1234. [CrossRef]
44. Janiak, C. A critical account on π–π stacking in metal complexes with aromatic nitrogen-containing ligands†. *J. Chem. Soc., Dalton Trans.* **2000**, 3885–3896. [CrossRef]
45. Desiraju, G.R. *Crystal Design: Structure and Function Perspectives in Supramolecular Chemistry*; John Wiley & Sons, Ltd.: Chichester, UK, 2003; Volume 7.
46. Nakamoto, K. *Infrared and Raman Spectra of Inorganic and Coordination Compounds*; Wiley: New York, NY, USA, 1986.

47. Vafazadeh, R.; Esteghamat-Panah, R.; Willis, A.C.; Hill, A.F. Synthesis and structural studies of mono- and dinuclear Cu(II) complexes with an ONO donor Schiff base ligand: Self-assembly and sulfato-bridged. *Polyhedron* **2012**, *48*, 51–57. [CrossRef]
48. Hathaway, B.J.; Billing, D.E. The electronic properties and stereochemistry of mono-nuclear complexes of the copper(II) ion. *Coord. Chem. Rev.* **1970**, *5*, 143–207. [CrossRef]
49. Lever, A.P.B. *Inorganic Electronic Spectroscopy*, 2nd ed.; Elesvier: Amsterdam, The Netherlands, 1984.
50. Fox, K.R. *Methods in Molecular Biology. Drug-DNA Interaction Protocols*; Humana Press: Totowa, NJ, USA, 2007.
51. Rajeshwari, K.; Anantha Lakshmi, P.V.; Archana, J.; Sumakanth, M. Ternary cobalt(II), nickel(II), and copper(II) complexes containing metformin and ethylenediamine: Synthesis, characterization, thermal, in vitro DNA binding, in silico molecular docking, and in vivo antihyperglycemic studies. *Appl. Organomet. Chem.* **2021**, *35*, e6100. [CrossRef]
52. Lepecq, J.B.; Paoletti, C. A fluorescent complex between ethidium bromide and nucleic acids. *J. Mol. Biol.* **1967**, *27*, 87–106. [CrossRef] [PubMed]
53. Valeur, B. *Molecular Fluorescence. Principles and Applications*; Wiley: Weinheim, Germany, 2001.
54. Christidou, A.; Zavalani, K.; Hatzidimitriou, A.G.; Psomas, G. Copper(II) complexes with 3,5–dihalogeno–salicylaldehydes: Synthesis, structure and interaction with DNA and albumins. *J. Inorg. Biochem.* **2023**, *238*, 112049. [CrossRef] [PubMed]
55. Housecroft, C.E.; Sharpe, A.G. *Inorganic Chemistry*, 2nd ed.; Pearson Education Limited: Harlow, UK, 2005.
56. Lakowicz, J.R. *Principles of Fluorescence Spectroscopy*, 2nd ed.; Kluwer Academic/Plenum Publishers: New York, NY, USA, 1999.
57. Urquiza, N.M.; Naso, L.G.; Manca, S.G.; Lezama, L.; Rojo, T.; Williams, P.A.M.; Ferrer, E.G. Antioxidant activity of methimazole–copper(II) bioactive species and spectroscopic investigations on the mechanism of its interaction with Bovine Serum Albumin. *Polyhedron* **2012**, *31*, 530–538. [CrossRef]
58. Chang, L.-l.; Yang, J.; Lai, S.-q.; Liu, X.-r.; Yang, Z.-w.; Zhao, S.-s. Synthesis, crystal structures and CT-DNA/BSA binding properties of Co(III) and Cu(II) complexes with bipyridine Schiff base ligand. *Inorg. Chim. Acta* **2022**, *532*, 120751. [CrossRef]
59. Nakahata, D.H.; de Paiva, R.E.F.; Lustri, W.R.; Corbi, P.P. Sulfonamide-containing copper(ii) complexes: New insights on biophysical interactions and antibacterial activities. *New J. Chem.* **2020**, *44*, 17236–17244. [CrossRef]
60. Sohtun, W.P.; Kathiravan, A.; Asha Jhonsi, M.; Aashique, M.; Bera, S.; Velusamy, M. Synthesis, crystal structure, BSA binding and antibacterial studies of Ni(II) complexes derived from dithiocarbazate based ligands. *Inorg. Chim. Acta* **2022**, *536*, 120888. [CrossRef]
61. Rajendiran, V.; Karthik, R.; Palaniandavar, M.; Periasamy, V.S.; Akbarsha, M.A.; Srinag, B.S.; Krishnamurthy, H. Mixed-Ligand Copper(II)-phenolate Complexes: Effect of Coligand on Enhanced DNA and Protein Binding, DNA Cleavage, and Anticancer Activity. *Inorg. Chem.* **2007**, *46*, 8208–8221. [CrossRef]
62. Kanchanadevi, S.; Fronczek, F.R.; Immanuel David, C.; Nandhakumar, R.; Mahalingam, V. Investigation of DNA/BSA binding and cytotoxic properties of new Co(II), Ni(II) and Cu(II) hydrazone complexes. *Inorg. Chim. Acta* **2021**, *526*, 120536. [CrossRef]
63. Neelakantan, M.A.; Balamurugan, K.; Balakrishnan, C.; Subha, L. Interaction of amino acid Schiff base metal complexes with DNA/BSA protein and antibacterial activity: Spectral studies, DFT calculations and molecular docking simulations. *Appl. Organomet. Chem.* **2018**, *32*, e4259. [CrossRef]
64. Bashir, M.; Yousuf, I.; Prakash Prasad, C. Mixed Ni(II) and Co(II) complexes of nalidixic acid drug: Synthesis, characterization, DNA/BSA binding profile and in vitro cytotoxic evaluation against MDA-MB-231 and HepG2 cancer cell lines. *Spectrochim. Acta A Mol. Biomol. Spectrosc.* **2022**, *271*, 120910. [CrossRef] [PubMed]
65. Damelin, L.H.; Vokes, S.; Whitcutt, J.M.; Damelin, S.B.; Alexander, J.J. Hormesis: A stress response in cells exposed to low levels of heavy metals. *Hum. Exp. Toxicol.* **2000**, *19*, 420–430. [CrossRef] [PubMed]
66. Fulmer, G.R.; Miller, A.J.M.; Sherden, N.H.; Gottlieb, H.E.; Nudelman, A.; Stoltz, B.M.; Bercaw, J.E.; Goldberg, K.I. NMR Chemical Shifts of Trace Impurities: Common Laboratory Solvents, Organics, and Gases in Deuterated Solvents Relevant to the Organometallic Chemist. *Organometallics* **2010**, *29*, 2176–2179. [CrossRef]
67. Bruker. APEX2. v2010.3-0. Bruker AXS Inc.: Madison, WI, USA, 2010.
68. Bruker. *SMART and SAINT. Area Detector Control and Integration Software*; Bruker Analytical X-ray Instruments Inc.: Madison, WI, USA, 1997.
69. Sheldrick, G.M. *SADABS. Program for Empirical Absorption Correction of Area Detector Data*; University of Goettingen: Goettingen, Germany, 1997.
70. Sheldrick, G.M. A short history of *SHELX*. *Acta Crystallogr.* **2008**, *A64*, 112–122. [CrossRef]
71. Wilson, A.J.C. *International Tables for Crystallography*; Kluwer Academic Publishers: Dordrecht, The Netherlands, 1995; Volume C.